

Received 9 February 2023, accepted 11 March 2023, date of publication 22 March 2023, date of current version 29 March 2023.

Digital Object Identifier 10.1109/ACCESS.2023.3260778



RESEARCH ARTICLE

Dynamics and Stability of Power Systems With High Shares of Grid-Following Inverter-Based Resources: A Tutorial

AMIRHOSSEIN SAJADI^{ID1}, (Senior Member, IEEE), JO ANN RAÑOLA², (Member, IEEE), RICK WALLACE KENYON^{ID1,3,4}, (Member, IEEE), BRI-MATHIAS HODGE^{1,3,4,5}, (Senior Member, IEEE), AND BARRY MATHER^{ID6}, (Senior Member, IEEE)

¹Renewable and Sustainable Energy Institute (RASEI), University of Colorado Boulder, Boulder, CO 80303, USA

²Integrated Grid and Energy Systems-Power Delivery and Utilization (IGES-PDU) Group, Electric Power Research Institute (EPRI), Palo Alto, CA 94304, USA

³Department of Electrical, Computer & Energy Engineering, University of Colorado Boulder, Boulder, CO 80309, USA

⁴National Renewable Energy Laboratory (NREL), Grid Planning and Analysis Center, Golden, CO 80401, USA

⁵Department of Applied Mathematics, University of Colorado Boulder, Boulder, CO 80309, USA

⁶National Renewable Energy Laboratory (NREL), Power Systems Engineering Center, Integrated Devices and Systems Group, Golden, CO 80401, USA

Corresponding author: Amirhossein Sajadi (Amir.Sajadi@colorado.edu)

This work was supported in part by the U.S. Department of Energy (DOE) Office of Strategic Programs titled: Power System Stability and Energy Efficiency & Renewable Energy (EERE) Technologies, under Agreement 25315; in part by the National Renewable Energy Laboratory, operated by Alliance for Sustainable Energy, LLC, for the DOE; and in part by the U.S. Department of Energy with the National Renewable Energy Laboratory under Contract DE-AC36-08-GO28308.

ABSTRACT Electric power systems worldwide are undergoing a foundational transition from mechanical-backed generation technologies dominating the resource mixture, primarily synchronous generators, into a hybrid system consisting of periods of a preponderance of power electronics-backed generation technologies, primarily solar photovoltaics and wind power plants and battery storage systems. Almost all current inverter-based resources integrated into bulk power systems are grid-following technology, and there exists a knowledge gap concerning the impacts of large-scale integration of grid-following inverters on power system dynamics, which is a critical aspect of power system planning and operation. This paper serves as a tutorial and addresses the stability and reliability challenges pertinent to the integration of grid-following interfaced inverter-based resources. While considering both small-signal and large-signal stability problems, it demonstrates and explains the underlying interrelated dynamics of electric angle, frequency, and voltage, as well as the impacts that system inertia can have on system stability. Industry-grade electromagnetic transient simulations in Power Systems Computer-Aided Design (PSCAD) are utilized to demonstrate the concepts presented in this paper, and all the computer models have been made available to the public at no cost.

INDEX TERMS Grid-following inverter, inverter-based resources, power system dynamics, renewable energy systems.

I. INTRODUCTION

Integration of variable renewable energy (VRE) technologies, mainly solar photovoltaic (PV) and wind, has been accelerating worldwide, in part due to environmental concerns and financial incentives for generation companies as well

The associate editor coordinating the review of this manuscript and approving it for publication was Nagesh Prabhu^{ID}.

as regulatory and public policies at the regional, state, and national level. Solar PV and wind power plants are now cost-competitive with conventional generation in most locations, and the cost of energy production using renewable power plants continues to decline [1]. In 2020, solar and wind resources globally accounted for more than 72% of all new electricity generation capacity [2]. This set a new record for the expansion of renewable installations by more than 45%

from 2019 [3]. It is expected that the VRE technologies will continue to dominate the newly installed power generation capacity around the globe, with solar and wind anticipated to account for approximately 90% of new generation capacity in 2021 and 2022 [4].

VRE power plants are commonly integrated into power systems with a power electronics inverter, commonly referred to as inverter-based resources (IBRs). A review of the literature reveals that IBR integration was embarked on in the 1980s [5], [6], [7], [8], [9] with the development of the power electronics inverters to serve as the interface between solar panels or wind turbines and the power grid. This progress continued into the early 2000s with the development of larger inverters with higher capacity with the application for solar or wind power plants [10], [11], [12], [13], [14], [15], [16], [17], [18]. At this point, the grid-following (henceforth referred to as GFL) inverters were commonly known as “grid-tie” or “grid-connected” inverters and were mainly studied at the device level and in microgrid applications. As the power electronics inverter reached sufficient maturity to integrate VRE into the power system at scale, the mass integration of IBRs into the power grid began, and so did the study of this problem at the system level [19], [20], [21], [22], [23], [24], [25], [26]. Subsequently, research began to uncover the adverse impact of the mass integration of GFL inverters on system stability and, therefore, the realm of “low-inertia” power systems was coined in early 2010s [21], [27]. In the meantime, parallel connected grid-forming technology which stemmed from the Consortium for Electric Reliability Technology Solutions (CERTS) Microgrid project [28], [29] started in 2006 as one of the earliest microgrid projects around the world. At that point, the dichotomy arose between research and practice where the academic research primarily shifted towards the integration of IBR integration via grid-forming (henceforth referred to as GFM) technology [30], [31], [32], [33], [34], [35], [36], [37], [38], [39], [40], [41], [42]. In contrast, in practice, almost universally, all new IBR installations have been GFL inverters. The parallel inverter technology, the GFM, is an emerging application, and its use in interconnected generation facilities at the moment is extremely limited.

Studies whose focus was on the integration of GFL-IBRs into power systems at the bulk scale were often empirical by relying on using computer models to develop a holistic understanding of the system with great attention to frequency response [19], [20], [22], [23], [24], [25], [26]. There is substantial complexity in the modeling of IBRs and the lack of sufficient and accurate data because of the lack of transparency by vendors tied to their proprietary designs. Understandably, there are also limitations to the power simulation platforms that make it challenging to draw analytical or scientific inferences solely based on empirical observations. This shortcoming has left a broad range of technical challenges unanswered, particularly regarding grids with high shares of

GFL-IBR devices and their interrelated dynamics between frequency, voltage, and electric angle. Recently, we studied dynamical interactions between GFL and synchronous generator (SG) at the device level [37], demonstrating that GFL can destabilize SG. The results from that paper were intriguing and motivated us to look further into this problem and produce the present paper.

A review of the state of the industry pertinent to the IBR integration directs us to the North American Electric Reliability Corporation (NERC) Inverter-Based Resource Performance Guideline [43], IEEE 1457 Standards [44], [45], and various modeling guidelines and standards for utilities [46], [47], [48], [49], [50], [51], which address operational requirements and characteristics of GFL-IBR with a focus on individual devices. These standards and guidelines are concerned with the IBR settings and functionality for transmission operators to include those details in their interconnection agreement with the generation facility. In recent years, several large-scale interruptions of power delivery attributed to the GFL-IBR have been observed [52], [53], [54], [55], [56]. The analyses of these events pointed at the miscoordination of GFL devices with the extant power system as the root cause. These blackout events have exposed the knowledge gap concerning the impacts of GFL-IBR integration on system dynamics, which is a critical aspect of power system planning and operation, particularly at scale.

This paper offers a review of the fundamentals of power system dynamics and stability and tailors it to the interactions between SGs and GFL-IBRs. The considerations are that SGs are equipped with an active governor while GFL-IBRs are without grid-supporting functionality. Throughout the paper, mathematical rigor is applied to the underlying governing physics and accompanied by several diagrams in parametric space along with corresponding time-domain response to better orient the reader.

The wholistic analysis offered in this paper addresses both the small-signal and large-signal stability. It covers a broad range of dynamic issues, including electric angle stability, frequency response, and voltage stability, and offers an insight into the interrelation among these complex dynamics. The analysis of the conventional power system with SG domination is well established in the literature and, thus, borrowed from Machowski [57] and Van Cutsem [58]. The analysis of GFL and the implications of integrating the two technologies are the new additions this paper offers to the body of literature hence it is the contribution of this paper.

To demonstrate the described dynamical phenomena and concepts, a 9-bus Western System Coordinating Council (WSCC) test case (also known as the Anderson 9-bus) has been developed in Power Systems Computer-Aided Design (PSCAD) with detailed (full-order) GFL-IBR models including the inner current loops and associated filter elements. PSCAD is a power system simulation platform that operates in an electromagnetic transient (EMT) timeframe that is effective at capturing the fast transients of power electronics.

The models developed for this study are open-source and available to the public at [59], and the model description is available in [60].

Six key demonstrations in this paper are as follows.

1) Replacing synchronous generators with grid-following inverter-backed generators can significantly compromise the stability of a power grid. This is mainly because of grid-following inverters lack of active participation in system power balance regulation; their mass integration can overwhelm the extant synchronous generators and overall make the system susceptible to instabilities.

2) Significant levels of grid-following inverter-backed generators could transform the frequent events that conventionally are understood and analyzed as small-signal stability problems (such as load switching or generation dispatch) into large-signal stability problems. Suppose the grid-following inverters do not support the grid during transients. In that case, they could force the trajectory of synchronous generators to move so drastically in response to a grid event such that events that are conventionally understood as small-signal stability problems could become large-signal stability events.

3) Displacement of synchronous generators effectively reduces the system's overall headroom reserve and deteriorates system frequency response and voltage stability. Further study is recommended to better understand the headroom reserve required for simultaneous active and reactive power support in order to maintain system reliability.

4) Replacing synchronous generators with grid-following inverter-backed generators can result in larger system frequency oscillations and deviation when subjected to a large disturbance. The reason for it is twofold. First, the reduced effective system inertia results in larger frequency oscillations during the grid events. Second, the aggregate system frequency droop value increases, exacerbating the frequency deviations and compromising the system ability to restore frequency.

5) The additional mechanical inertia provided by synchronous generators improves system transient stability. This is because of the lack of fast responding resources to compensate for more agile dynamics if the extant synchronous generators are displaced.

6) We observed chaotic motions in the system frequency response during very low inertia operating conditions which require further investigation. We could not make a definite determination about the root cause of this phenomenon. Still, our understanding suggests that these chaotic motions could be linked to the interaction of phase locked loops or the blind injection of power by grid-following inverters into the grid regardless of grid status.

II. DYNAMICS AND STABILITY IN POWER SYSTEMS

Analysis of the dynamic behavior and stability of the power system is the foundation for a wide range of processes and procedures in power system planning, operation, and control. The impetus of such analysis is to understand whether a

system is stable in a particular steady state and if it remains stable following a disturbance. It characterizes the system response and identifies equilibria and their individual stability conditions that collectively determine the stability of entire system. Small-signal stability analysis refers to the investigation of system stability when subjected to a small disturbance within the linear regime that does not result in a change of system topology, e.g., load switching or a binary generation dispatch change. Large-signal stability analysis refers to the investigation of system stability when subjected to a large disturbance that results in changes in system topology, e.g., electrical faults or the loss of components such as lines or generation units.

The critical state variables in the analysis of dynamics and stability of power systems are: (1) electric angle, (2) frequency, and (3) voltage. The remainder of this section discusses the three primary dynamic subcategories and delves into them.

A. ELECTRIC ANGLE STABILITY

Electric angle stability is concerned with the stability of individual generators, which is foundational to a synchronized operation, given that a realistic power system is continuously subject to disturbances. The synchronized operation of a power system manifests as a homogeneous frequency at all busbars across the system (e.g., 60 Hz in North America and 50 Hz in Europe). The system-wide frequency, f_s , defines the synchronization speed, $\omega_s = 2\pi f_s$. Synchronization speed is an electric variable measured in electrical radians per second. In a synchronized power system, the synchronization speed of all generators across the system is identical; in a power system with n -generators, it can be mathematically described by [61]:

$$\dot{\delta}_1 = \dot{\delta}_2 = \dot{\delta}_3 = \dots = \dot{\delta}_n = \omega_s = 2\pi f_s \quad (1)$$

where δ_i , $i = 1, 2, \dots, n$, represents the electric angle of the i th generator, and the dot notation indicates the time derivative $\dot{x} = \frac{dx}{dt}$. In conventional power systems where SG is the primary technology for power generation, synchronization speed is related to the rotor mechanical speed, and the electric angle is related to the rotor mechanical angle. In GFL interfaced generators, this electric angle is generated by the phase locked loop (PLL) using a real-time estimation of the grid frequency at the interconnection point.

In a steady state, generator electric power output (P_e) can be described as a function of its electric angle (δ) by:

$$P_e = \frac{EV}{X} \sin\delta \quad (2)$$

where E and V are the voltage behind reactance and the terminal voltage of the generator, respectively, and X is the generator reactance for an SG. For GFL, E and V are the voltage at the output of power electronics switches and the terminal voltage (output of filter), respectively, and X is the filter effective reactance. At equilibria, input power, P_{m_i} , (mechanical in SG and electrical in GFL) and output electric

power, P_e , are equal, and thus, it can be expressed, $P_{m_i} = P_{e_i}$, geometrically identified as the intersection of P_m and P_e characteristics. P_m determines the available headroom power for the generator and P_e is the generator characteristic that relates the electric power output and electric angle. The peak of this characteristic is the critical power output. Fig. 1 depicts this characteristic and associated equilibria. As shown in this plot, there exist two solutions if P_{m_i} is below critical power output, only one of which is stable. If P_{m_i} is equal to the critical power output, then there exists a critically stable solution. If P_{m_i} is greater than the critical power output, then no solution exists.

Small-Signal Stability: With SG, once a disturbance is detected by frequency deviation, the governor adjusts the mechanical power generation to cover the transient electric power imbalance, and if sufficient headroom is available, and returns the electric speed to its equilibrium. The set of linear equations that describe the dynamics of SG is [57]:

$$\Delta\dot{\omega}_i = \frac{1}{M_i}(\Delta P_{m_i} - \Delta P_{e_i} - \Delta P_{d_i}) \quad (3)$$

$$\Delta\dot{\delta}_i = \Delta\omega_i \quad (4)$$

where M_i is the inertia coefficient of the i th generator and P_{m_i} , P_{e_i} , and P_{d_i} are the mechanical input, electrical output, and damping power (provided by the damper windings), respectively, and Δ is the operator for deviation from a steady state value.

On the other hand, GFL interfaced generator does not regulate its electric angle and, thus, does not construct frequency. Therefore, its control objective is to maintain the power generation to the pre-disturbance setpoint. Its power balance can be defined by:

$$0 = \Delta P_{c_i} - \Delta P_{e_i} - \Delta P_{d_i} \quad (5)$$

where P_{c_i} , P_{e_i} , and P_{d_i} are i th generator input electrical power through the filter, output electrical power to the grid, and power loss (generally negligible), respectively. The governing equation for GFL interfaced generators is merely algebraic; therefore, in system-level studies, they can be treated as a negative constant load at low shares.

If the loading condition of an SG is changed, then the system equilibria move on this $P - \delta$ plane. With sufficient mechanical power headroom, the governor adjusts the mechanical power to achieve a new equilibrium point. Suppose $P_{m_2} > P_{m_1}$. When the generator is disturbed, the governor will increase the working fluid intake to increase mechanical power and match the new electrical power output. This causes the rotor to accelerate and gain momentum and drives the system trajectory towards the new set point P_{m_2} . Because of the momentum, the trajectory may pass the new mechanical power set point where the electrical power becomes greater than the mechanical power momentarily ($P_e > P_m$) again, the rotor is forced back towards the equilibrium point [57], creating a converging spiral that eventually settles at the new equilibrium point. The movement of system trajectory in the $P - \delta$ plane for changing loading conditions of an SG is shown in Fig. 2(a).

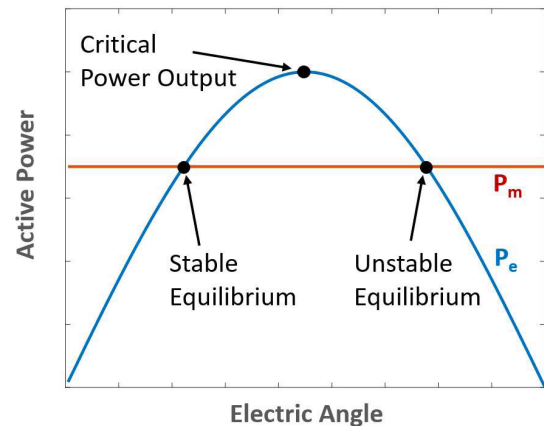


FIGURE 1. Illustration of solutions of the system and a $P - \delta$ characteristic.

Suppose the loading condition of a GFL interfaced generator is changed. In that case, the power output may momentarily experience transient oscillations and small export drops, not because of grid-supporting response, but mainly because of temporary low voltage conditions or voltage oscillations which could tamper with the power output as well as potentially calculation error induced by the PLL. In fact, GFL will not change its output power set point at all. If the oscillations are damped out by support from the other generation units, the inverter will maintain its operation at its pre-disturbance power output set point. Otherwise, sustained oscillations can interfere with GFL devices and force them to the malfunction. The movement of the system trajectory in the $P - \delta$ plane for changing loading conditions of a GFL interfaced generator is shown in Fig. 2(b).

Large-Signal Stability: If a generator is subjected to a large disturbance that would result in the migration of its state outside the pre-disturbance equilibrium neighborhood, then the linear approximation assumed for small-signal stability analysis is no longer holds valid. Generally, such disturbances are electric short-circuits or the disconnection of the line(s). These events produce large transient dynamic excursions because of the changes in network equivalent impedance during and following the disturbing event relative to the pre-disturbance operation. As a result, the power balance between generation and consumption is often significantly disturbed under a very short period. Consequently, the system can be immensely stressed, resulting in loss of synchronization and, hence, instability. The set of equations that describe the rotational dynamics of SG is [57]:

$$\dot{\omega}_i = \frac{1}{M_i}(P_{m_i} - P_{e_i} - P_{d_i}) \quad (6)$$

$$\dot{\delta}_i = \omega_i \quad (7)$$

where M_i is the inertia coefficient of the i -th generator and P_{m_i} , P_{e_i} , and P_{d_i} are the input, electrical output, and damping power (provided by the damper windings), respectively. For the sake of simplicity and clarity of the analysis here, the

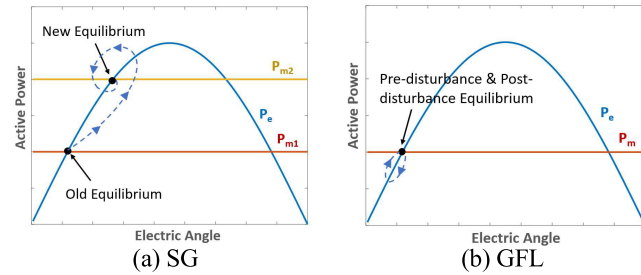


FIGURE 2. Illustration of system trajectory on the $P - \delta$ plane after a change in loading condition of SG and GFL.

generator damping power, P_{d_i} , can be neglected (generally, it is a very small value).

In a steady-state, pre-disturbance operation, the mechanical output power is equal to the electric output power, $P_{m_i} = P_{e_i}$. As an electrical fault occurs in the network, the equivalent network impedance changes, which causes a change in electrical power consumption. Subsequently, the electric output power, P_{e_i} , changes. In this situation, the equation that describes the system dynamic of an SG is:

$$\ddot{\delta}_i = \frac{1}{M_i}(P_{m_i} - P_{e_i}) \quad (8)$$

The closer the electric proximity of the electrical fault to the generator terminal, the more severe the ramifications are. The worst-case scenario is a three-phase electrical fault at a generator terminal where the electric output power of that generator will plunge to zero, $P_{e_i} = 0$. In this particular situation, the equation that describes the system dynamic of SG is:

$$\ddot{\delta}_i = \frac{P_{m_i}}{M_i} \quad (9)$$

When the fault is on, the electric speed increases, which is found by integrating $\ddot{\delta}_i$ with respect to time. It produces

$$\omega_i = \dot{\delta}_i = \frac{P_{m_i}}{M_i}t \quad (10)$$

A second integration produces electric angle trajectory as a function of time:

$$\delta_i(t) = \frac{P_{m_i}}{2M_i}t^2 + \delta_{i_0} \quad (11)$$

where δ_{i_0} is the initial electric angle. These equations show that from when the fault occurs until it is cleared, the electric speed increases linearly with time and the electric angle increases proportionally to the square of time.

When the fault is successfully cleared and system retained its stability, the electric power output will arrive at a post-fault equilibrium, which could be the pre-disturbance value or a new value. During the fault, the rotor acceleration causes the electric angle to increase until the fault clears, and then the resultant rotor kinetic energy should be dissipated before settling at its final value. Fig. 3(a) visualizes the system trajectory on the $P - \delta$ plane. The longest duration of a fault that following a clearance the system would be able to regain

its stable and synchronized operation is called the critical clearance time (CCT). If the fault is cleared before the CCT, the generator power and angle values will return to stable values after the transient oscillations are damped out.

Suppose a three-phase electrical fault occurs within close electric proximity of a GFL interfaced generator terminal. In that case, the voltage is greatly reduced, and the electric output power of the generator plunges significantly, which might lead to momentary cessation and/or blocking. Let us suppose a worst-case scenario where output power drops to zero, $P_{e_i} = 0$. Subsequently, the generator electrical output power through the filter goes to zero, $P_{m_i} = 0$. Once the fault is cleared, provided that the device functional safety permits, the generator attempts to regain the pre-disturbance electric output power, as shown in Fig. 3(b). If the electrical fault is cleared before the CCT, the generator power and angle values will return to their pre-disturbance values after the transient oscillations are damped out.

B. FREQUENCY RESPONSE

The momentary mismatch of active power generation and consumption and active power oscillations can produce transient frequency excursions and oscillations. The response of each generator to active power transient oscillations and power output adjustments depends on its power-frequency characteristic, commonly known as the frequency droop characteristic. It relates each generator change in generator active power to cover the overall system power deficit as a function of system frequency. Fig. 4. depicts a typical frequency-droop characteristic. The participation extent of a generator in covering for power deficit is governed by its droop factor (λ), which establishes the relationship between the generator active power change as a function of frequency deviation and geometrically is the slope of power-frequency characteristic. As shown in this plot, the ability of a generator is physically constrained by its available headroom reserve (the difference between the actual generation set point and the maximum capacity).

Small-Signal Stability: Following a small grid event, e.g., load switching, all grid-supporting generators participate to compensate for the power deficit, P_l

$$P_l = \sum_i \lambda_i^{-1} \Delta P_i \quad (12)$$

where λ is droop factor of i th generator and ΔP_i is the change in its power output.

When the loading condition of an SG changes, then the frequency departs from its equilibrium and manifests itself in the form of a frequency deviation in the time-domain. If headroom mechanical power is available, the governor adjusts the mechanical power to achieve a new equilibrium point. This is known as primary frequency control. Although the values of droop could vary, in North America, it is commonly set at 5% ($\lambda = 0.05$). The movement of the system trajectory in the $P - f$ plane for changing loading conditions of an SG is shown in Fig. 5(a).

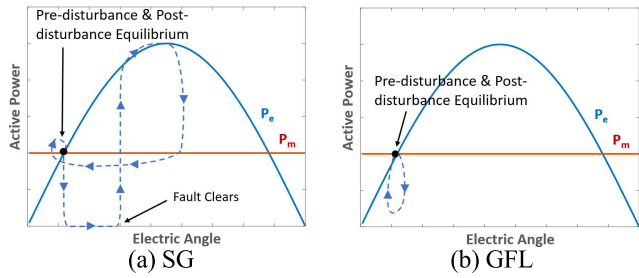


FIGURE 3. Illustration of trajectory on the $P - \delta$ plane after an electrical fault with a successful clearance for SG and GFL.

If the system loading condition changes, non-grid supporting GFL interfaced generators do not adjust their power output to cover the power deficit or surplus. Instead, the pre-disturbance value of power output remains. As a result, the droop value of a GFL interfaced generator is infinite, $\lambda = \infty$, meaning that it does not participate in frequency regulation. The movement of the system trajectory in the $P-f$ plane for a change of loading condition of a GFL interfaced generator is shown in Fig. 5(b).

Let us consider a small power system encompassing only two SGs with identical capacities and droop factors. If this system is subjected to a change of loading condition equivalent to ΔP , then both generators adjust their output power to cover the power deficit. The resultant system frequency change, Δf , is determined by the droop factor whilst the rate of change of frequency (ROCOF) is directly determined by the system inertia, as shown in Fig. 6(a). Now, suppose one of the two SGs is replaced by a GFL interfaced generator whose capacity is identical to that of the expelled SG, and the new system is subjected to the same change of loading condition equivalent of ΔP . In that case, only SG will adjust its output power to cover the power deficit, and GFL interfaced generator will not. The subsequent resultant system frequency change is larger than the previous scenario (in this case, doubled) because of the increased effective system droop factor, and the resultant ROCOF is larger (also doubled) because of reduced system inertia, as shown in Fig. 6(b). It should be noted that following small grid events, the main concern is the availability of sufficient headroom reserve for ensuring frequency stability and restoration. In the time-domain, the larger resultant frequency deviation in the latter scenario (with an SG and one GFL interfaced generator) produces a lower nadir frequency and larger frequency deviation, almost twice as much as in the former scenario (with two identical SGs), as shown in Fig. 7.

Large-Signal Stability: When an electrical fault occurs within close electric proximity of an SG, the active output power plunges, and, subsequently, system frequency could rise. It was established that when the fault is on, the electric speed increases by:

$$\omega_i = \dot{\delta}_i = \frac{P_{m_i} - P_{e_i}}{M_i} t \quad (13)$$

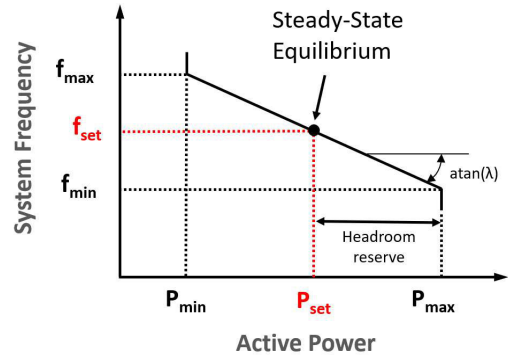


FIGURE 4. Illustration of a $P - f$ characteristic for a generator ($\text{atan}(\lambda)$ is inverse tangent).

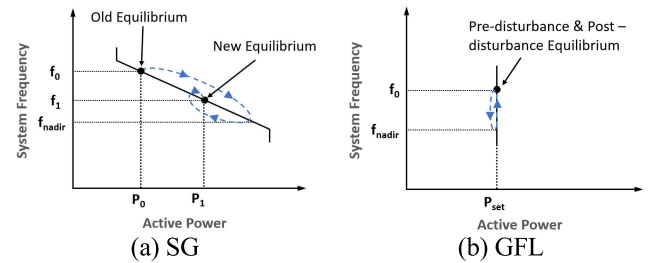


FIGURE 5. Illustration of system trajectory in the $P - f$ plane after a change in loading condition of SG and GFL.

Knowing that $\omega_i = 2\pi f_i$, then the frequency, which is the generator electric speed and directly tied to the mechanical speed of SG, the increase can be described by:

$$f_i = \frac{P_{m_i} - P_{e_i}}{2\pi M_i} t + f_n \quad (14)$$

where f_i is the frequency of the i th generator during the fault and P_{m_i} , P_{e_i} , and M_i are the mechanical and electrical power and inertia value, respectively, t is the duration of fault, and f_n is the nominal frequency. The frequency increase is proportional to the fault duration and the mechanical power. If the fault is cleared within the CCT, as shown in Fig. 8(a), the generator attempts to regain a stable operating condition. The rotor acceleration during the fault forces the active power beyond its settling value, and, as a result, the frequency deviates. However, in a SG-dominated power system, the frequency deviates at a moderate pace because of the present mechanical inertia of the rotor. In the mechanical sense, when the fault is cleared within the CCT, the rotor experiences a deceleration torque forcing it to slow down and, hence, the frequency declines. When the rotor kinetic energy is dissipated, the frequency and active power settle at a stable condition, which could be the pre-disturbance values or new post-fault values. Two factors are critical in the transient frequency stability of an SG: (1) the mechanical inertia that determines the pace at which frequency deviates, both the initial frequency increase and the subsequent frequency decline and (2) the droop response, which provides damping support

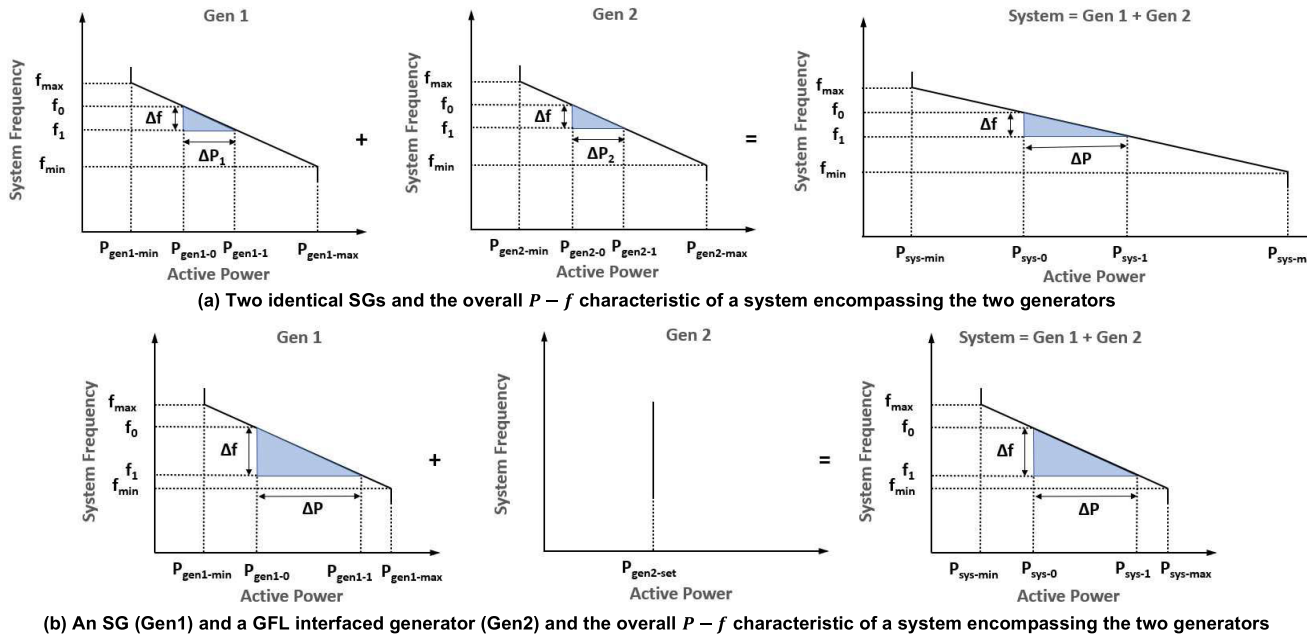


FIGURE 6. Illustration of $P - f$ characteristic of individual generators and the overall system.

to stabilize frequency oscillations and constitutes frequency restoration.

When an electrical fault occurs within close electric proximity of a GFL device terminal, the active output power plunges immediately, and so does the frequency. The frequency decline should be consistent with the system-level frequency behavior. However, because of voltage suppress and PLL error, the frequency profile in GFL may be registered with significant spikes and momentary transients, resulting in a significantly lower nadir frequency than the nadir frequency that an SG of similar capacity would produce. If the fault is cleared with the system CCT, GFL interfaced generator attempts to regain its pre-disturbance operating condition and the nominal frequency value. Immediately after the fault clearance, GFL device attempts to restore its normal operation, provided that the device functional safety permits, as shown in Fig. 8(b). It should be noted that during the frequency restoration, the PLL error can again produce a frequency spike (especially in larger power plants), as reported in [62].

Recall the two systems discussed in the small-signal stability analysis section. The first system consisted of two identical SGs, and the second system consisted of only one of the two SGs and a GFL interfaced generator whose capacity is identical to that of the expelled SG. If both systems are subjected to the same three-phase fault with a successful clearance within their CCT, the resultant system frequency oscillations are larger in the second system than in the first system. The reason is the reduced effective system mechanical inertia which results in a larger frequency excursion and exacerbated oscillations during transient operation, as shown in Fig. 9. Additionally, the aggregate system frequency droop

value in the second system increases because the introduced GFL does not offer grid supporting functionality in the form of frequency response, reducing the ability of system to restore its frequency if a fault results in a mismatch of power generation and consumption, e.g., loss of a generator.

C. VOLTAGE STABILITY

Changes in the system loading condition can also induce voltage oscillations. Following a disturbance, the voltage can experience transient oscillations. If these transients are not properly damped out, they can build up a sustained voltage drift, resulting in voltage collapse. The voltage transients mainly stem from the momentary mismatch of power that a disturbance can produce. Accordingly, the system capability to regulate voltage and bring it to steady (to prevent sustained voltage oscillations which are the root cause of voltage collapse) depends upon the capability of the generators to provide reactive power. At the same time, the active power demand must also be met. The active power transfer in a line is similar to the expression used for SG power injection and shown in Eq. (2) as $P = \frac{EV}{X} \sin\delta$, and the reactive power transfer could be described by $= \frac{EV}{X} \cos\delta - \frac{V^2}{X}$, both assuming $\frac{X}{R} \gg 1$ for simplicity and that all active and reactive power in the system is supplied by the generators (no other supporting devices such as capacitor, static Var compensator, etc). Applying the Pythagorean trigonometric identity equation to the angle produces [57], [58]:

$$(V^2)^2 + (2QX - E^2)V^2 + (PX)^2 + (QX)^2 = 0 \quad (15)$$

This is a second-order polynomial with respect to V^2 , whose solutions, assuming the necessary conditions for the

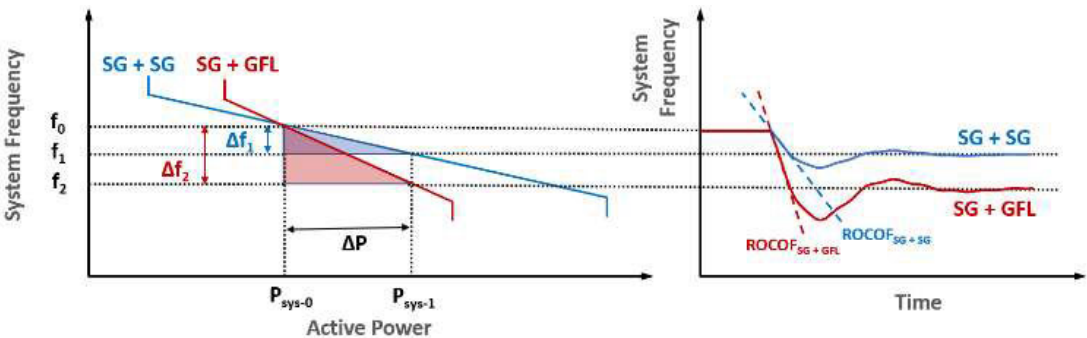


FIGURE 7. Illustration of the $P - f$ characteristic of two scenarios considered and the time-domain frequency response. It is evident that the replacement of SG with GFL interfaced generators results in higher ROCOF and lower nadir frequency.

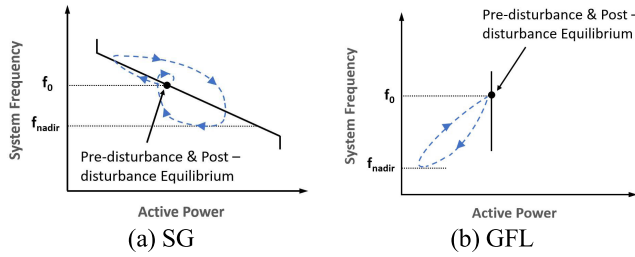


FIGURE 8. Illustration of system trajectory on $P - f$ after an electrical fault with a successful clearance for SG and GFL.

existence of its solutions holds valid, are [58]:

$$V_{1,2} = \sqrt{\frac{E^2}{2} - QX \pm \sqrt{\frac{E^4}{4} - X^2P^2 - XE^2Q}} \quad (16)$$

The plot of the two solutions for V as a function P yields two branches that coalesce at the bifurcation point, commonly known as a nose point. A family of these curves for different power factors is shown in Fig. 10(a). Of the two solutions, the system eigenvalues are such that only the upper branch is stable, and the lower branch is always unstable and not operational. This plot is the $P - V$ characteristic of a power system. Now, replacing the trigonometric functions with P and Q expressions produce the behavior of reactive power as follows [57]:

$$Q = \frac{1}{X} \sqrt{E^2V^2 - (PX)^2} - \frac{V^2}{X} \quad (17)$$

The plot of this description for Q as a function of V creates an inverted parabola where for each value of Q , two solutions for V may exist. A family of these curves for different power factors is as shown in Fig. 10(b). Of the two solutions, the system eigenvalues are such that only the right branch is stable, and the left branch is always unstable. This plot is the $V - Q$ characteristic of a power system.

Small-Signal Stability: At a steady state, the operating point of the generator determines the terminal voltage and active and reactive power. If the loading condition changes the voltage may temporarily fluctuate because of the power mismatch between the generation and demand. In the case of SG,

as it adjusts the mechanical power and follows the excitation system action, the operating point migrates along the trajectory according to active and reactive power adjustments and approaches the new equilibrium characteristics that reflect the new power factor (which is directly a function of the amount of active and reactive power switched). Subsequently, the voltage recovers. During the power adjustment process, momentarily, the generation trajectory may pass the settling equilibrium because of the generator mechanical momentum, creating voltage transients [57]. Then counteracting torque and damping elements aid the generation trajectory to reach its new equilibrium. Fig. 11 depicts typical $P - V$ and $V - Q$ curves for SG and the movement of system trajectory if the loading condition is changed.

As the loading conditions change, GFL will attempt to maintain its pre-disturbance power output. The transients from the network could impact GFL operation and, subsequently, voltage deviations could result in a temporary power drop. The movement of system trajectory in the $P - V$ and $V - Q$ planes for changing loading conditions of a GFL interfaced generator is shown in Fig. 12.

Large-Signal Stability: If an electrical fault occurs within close electric proximity of an SG, supposing the terminal, the electric output power immediately plunges to near zero, and the voltage significantly drops too for the entire duration of the fault. In the meantime, SG could temporarily increase the reactive output power due to exciter action and the voltage differentials for the entire fault duration to provide voltage support and avoid voltage collapse. Once the fault is cleared, the generator attempts to regain a stable power output value. But because of rotor acceleration and momentum gain during the fault, the system trajectory could be forced to move beyond its settling value along the $P - V$ and $V - Q$ characteristics until the deceleration torque dissipates the rotor kinetic energy, as shown in Fig. 13. If the fault is successfully cleared within the CCT, the output power and voltage will regain stable values, which could be their pre-disturbance equilibria or a new post-disturbance equilibrium, after oscillations are damped out.

If a three-phase electrical fault occurs within close electric proximity of a GFL interfaced generator terminal, the voltage

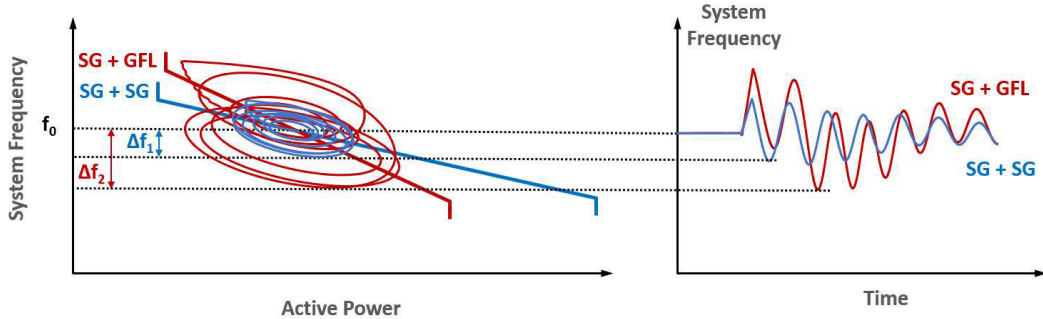


FIGURE 9. Illustration of $P - f$ characteristic of two scenarios considered and the time-domain system frequency response. It is evident that displacement of SG results in lower nadir frequency and larger frequency oscillations.

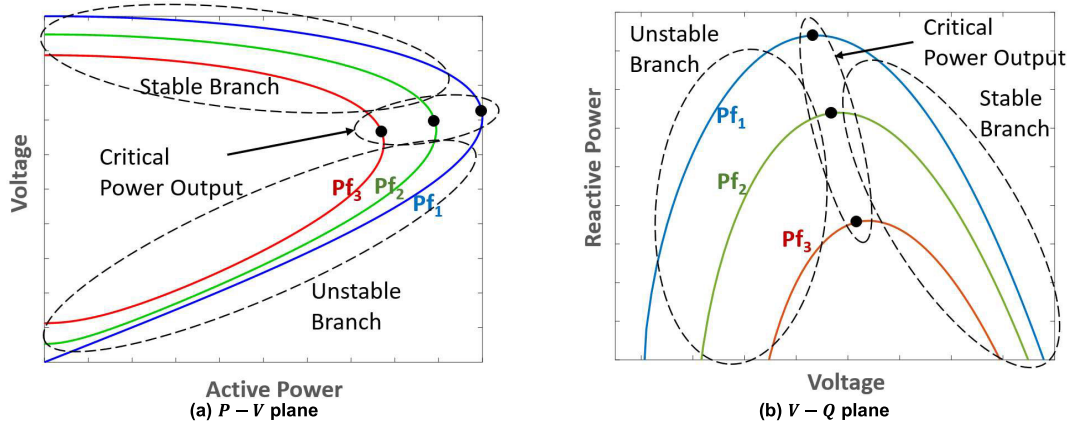


FIGURE 10. Illustration of solutions of the system in the $P - V$ and $V - Q$ planes for various power factors.

will plunge first, resulting in a subsequent plunge of electric output active and reactive power of the generator. This could cause a complete shutdown of GFL, e.g., momentary cessation. Once the fault is cleared within the system CCT, the GFL interfaced generator will attempt to regain its pre-disturbance operating condition, providing the device functional safety permits. During the restoration process, because of the potential PLL error, there could exist a transient overvoltage which is often damped very quickly, as shown in Fig. 14.

III. CASE STUDY AND SIMULATION METHODOLOGY

This section describes the details of this case study and the computer modeling methodology and assumptions.

A. TEST CASE: WSCC 9-BUS

This study uses the WSCC 9-bus system as a test case to demonstrate the stability concepts discussed in the previous section. The modified WSCC 9-bus test system consists of three-generation sources and nine high voltage transmission lines (see Fig. 15). Buses 4-9 are at 230 kV level. The generation buses 1-3 are at 16.5 kV, 18.0 kV, and 13.8 kV levels, respectively. All SG or GFL devices are rated at 200 MVA. The load is modeled as constant power with no frequency or voltage dependence.

To model GFL and, a set of open-source PSCAD models are used to represent IBRs accurately and transparently in the

EMT domain. Detailed structures of SG and GFL inverter are provided in Appendix I. A detailed description of these EMT models in PSCAD and their verification is available in [60]. The models used here, including the IBR, the network, and all associated static elements, are entirely editable and publicly available from the PyPSCAD NREL GitHub page [59]. The parameters of transmission lines and generators are provided in Appendix II.

B. MODELING IMPLEMENTATION

First, the load and generation dispatch datasets were generated using the power flow function in MATPOWER [63]. The power flow data was used to initialize the EMT dynamic simulations. Subsequent power system dynamic simulations were carried out using PSCAD 463 (64-bit), which is well-suited for modeling power electronics apparatus because it captures all fast transients and models three phases individually. Before the perturbation, the system is brought to a steady state by initiating all devices as ideal sources and then systematically releasing the associated dynamics in a manner conducive to maintaining steady-state stability; see [62] for additional PSCAD start-up methodology.

The duration of each EMT simulation is 20 seconds with step size of 1 millisecond, comprising 10 seconds pre-event for initialization and 10 seconds post-event to capture the transient dynamics resulting from the disturbance. This

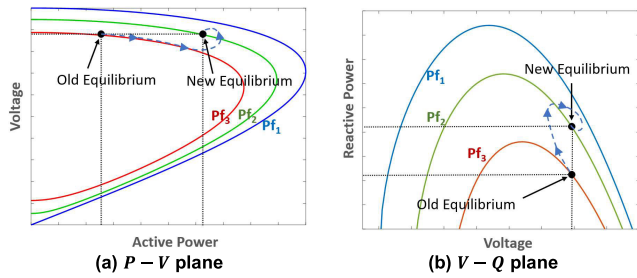


FIGURE 11. Illustration of system trajectory on the $P - V$ and $V - Q$ planes after a change in loading condition of an SG.

duration is long enough to determine whether the system remains stable. Following the event, the generators dynamic responses, including electric angles, speeds, power generation, and voltage profiles, were recorded and analyzed.

C. OPERATIONAL SCENARIOS CONSIDERED

The base case scenario in this study assumes all generation units to be SG, labeled as case “All SG”. Six cases were created to study the implications of replacing SGs with IBRs: GFL1, GFL2, GFL3, GFL12, GFL13, and GFL23. The numbers at the end of each subsequent case indicate the location of SG that is replaced by a GFL inverter interfaced generator of equal generation capacity. For example, GFL1 should be read as the case where SG attached to bus 1 is replaced with a GFL, and GFL12 indicates that SGs located in bus 1 and bus 2 are replaced with GFLs.

Small-Signal Stability: A small load switching event at bus 6 was used as the perturbation for small-signal stability analysis (highlighted in red at Load 2 in Fig. 15).

Large-Signal Stability: A three-phase balanced electrical short-circuit event (as the worst-case scenario) at bus 1 was used as the perturbation for the large-signal stability analysis (highlighted in red at Bus 1 in Fig. 15).

IV. SMALL-SIGNAL STABILITY ANALYSIS AND DISCUSSION

This section presents the results from small-signal stability analysis and discusses the findings in the following order: (a) electric angle stability, (b) frequency response, and (c) voltage stability.

A. ELECTRIC ANGLE STABILITY

In the base case, with all generation units being SG, when the system is subjected to a load switching event, all SGs participate in covering the power imbalance by increasing the mechanical power. In this study, SGs were considered to have sufficient headroom reserve to cover a 3 MW per phase power deficit, a total of 9 MW. The response from generators for active power adjustment is that each increases its output by approximately 3 MW, a total of 9 MW which is equivalent to the power imbalance created by load switching. The time-domain responses are depicted in Fig. 16(a).

GFL devices considered in this work do not offer any headroom reserve and only aim to maintain the power delivery at

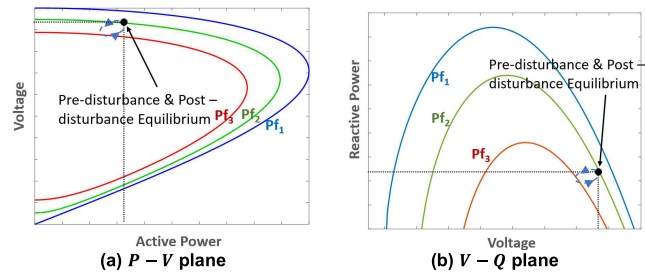


FIGURE 12. Illustration of system trajectory on the $P - V$ and $V - Q$ planes after a change in loading condition of GFL interfaced generator.

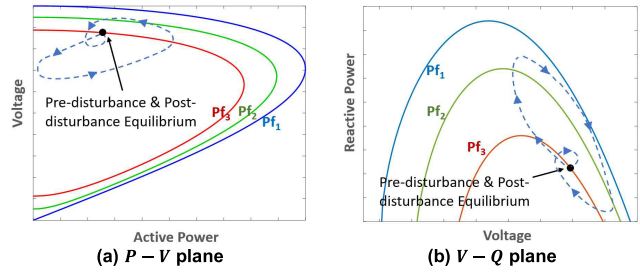


FIGURE 13. Illustration of system trajectory on $P - V$ and $V - Q$ planes of an SG after an electrical fault with a successful clearance.

the set point. To demonstrate the changes in system dynamics, all cases with IBR replacement were also subjected to a 3 MW load change per phase, a total of 9 MW. The results for a single IBR case, GFL1, and a double IBR case, GFL12, are presented in Fig. 16(b) and 16(c). The results from other single cases were similar to that of GFL1, and the results from other double IBR cases were similar to that of GFL12 were, and therefore are not shown.

In both single and double IBR cases, the support to cover the power imbalance was provided only by SGs, and GFLs did not participate. In GFL12, the adjustments by SG2 and SG3 were equally 4.5 MW, a total of 9 MW, while in GFL12, the adjustment by SG1 was 9 MW. The results for power output adjustment from all cases are summarized in Table 1.

The results consistently conclude that replacing SGs with IBRs can diminish available headroom reserve and system ability to cover the power imbalances. This phenomenon is because of GFL's lack of participation in system power balance regulation. It can also stress the remaining SGs in the system and force larger changes in the output of SGs, which inherently results in larger swings. Larger swings and smaller headroom reserve available, collectively, can diminish system stability margin because SG is forced to increase its output to cover the deficit to a greater extent making it closer to the critical power output.

Fig. 17 shows the $P - \delta$ characteristics of the generator connected to bus 2 (Gen 2) for four cases. The selection of Gen 2 and the four cases are an arbitrary choice and only for comparative demonstration purposes. The characteristics of other generators and other cases are similar and hence not shown. The cases indicated in this plot demonstrate four distinct operating conditions associated with the replacement of SG with GFL, as shown in Table 2.

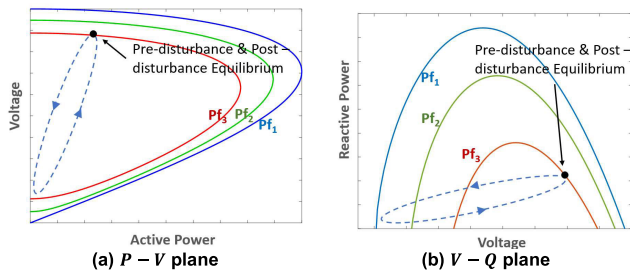


FIGURE 14. Illustration of system trajectory on $P - V$ and $V - Q$ planes of a GFL after an electrical fault with a successful clearance.

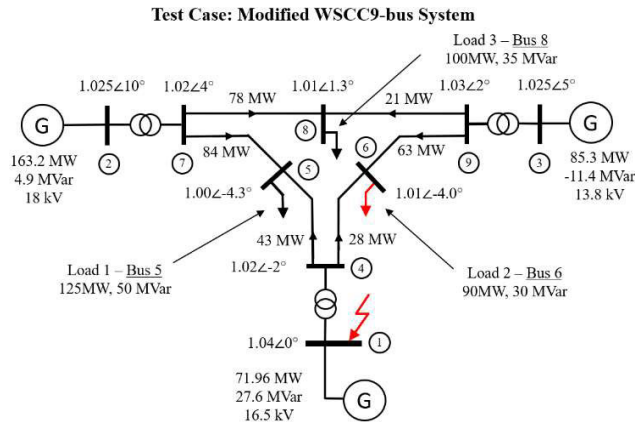


FIGURE 15. One-line diagram of the case study used for the stability analyses.

In the All SG case, where all three generators are SG, the output power of Gen 2 only moves by 3 MW from 163 MW to 166 MW because all three generators participate equally in covering the power deficit of 9 MW in this demonstration (see the blue trace in Fig. 17). In the GFL1 case, where only Gen 2 and Gen 3 equally participate in covering the 9 MW power deficit, Gen 2 moves by 4.5 MW from 163.5 MW to 168 MW (see the red trace in Fig. 17). In the GFL2 case, where Gen 2 does not participate in covering the power deficit, it can be seen that Gen 2 returns to its pre-disturbance set point after a minor transient swing (see the yellow trace in Fig. 17). In the GFL13 case, where only Gen 2 covers the 9 MW power deficit, Gen 2 adjusts its output by about 9 MW from 164 MW to approximately 173 MW (see the purple trace in Fig. 17), moving its trajectory closer to the critical power output. The observations here suggest a potential system reliability challenge with GFL-IBR replacing SGs.

The key takeaway in this observation is the critical role of available headroom reserve and the participation of generators in maintaining system stability. Another observation is that the lowest level of oscillations is seen in GFL13, which is attributed to the lowest inertia among all the cases analyzed, but the highest swing because of lack of support from GLFs.

B. FREQUENCY RESPONSE

Replacement of SGs with GFLs can also modify the system frequency response. This phenomenon is mainly because of the inability of GFL to adjust their output to compensate

for power imbalances effectively reduces the system headroom reserve and the ability to regulate frequency. System frequency response in the All SG, GFL1, and GFL12 cases when subjected to 9 MW load switching at bus 6 is shown in Fig. 18.

In the All SG case, the frequency decline is quite moderate and all three SGs maintain their synchronization throughout the transient operation. In the GFL1 and GFL12 cases, GFL exhibit large frequency transients immediately following the disturbance. This is because of the PLL error, consistent with the observation in field measurements in the Hawaiian power system [62]. Consistently for both IBR cases, the ROCOF was increased relative to the base case, and the nadir and settling frequencies were below their values in the base case. In the double IBR case, the increase in ROCOF was greater than the increase in the single IBR case, and the nadir and settling frequencies dropped further below their values in the single IBR case. The results from other single cases were similar to that of GFL1 and the results from other double IBR cases were similar to that of GFL12 and, therefore, not shown. The results for frequency response from all cases are summarized in Table 3.

Table 3 suggests a direct correlation between the SGs and the system nadir and settling frequencies—the more SGs in operation, the closer to nominal values the nadir and settling frequencies. To investigate this relationship, Fig. 19 shows the $P - f$ characteristics of the generator connected to busbar 2, described in Table 2.

In the All SG case, where all three generators are SG, the frequency drops from 59.97 Hz to 59.89 Hz (0.08 Hz excursion) and eventually settles at 59.92 Hz (see the blue trace in Fig. 19). In the GFL1 case, where only Gen 2 and Gen 3 equally participate in covering the 9 MW power deficit, the frequency drops from 59.97 Hz to 59.85 Hz (0.12 Hz excursion) and eventually settles at 59.90 Hz (see the red trace in Fig. 19), a level lower than the All SG case. In the GFL2 case, where Gen 2 does not participate in covering the power deficit, the observation is similar to the GFL1 case, where the frequency drops from 59.97 Hz to 59.86 Hz (0.11 Hz excursion) and eventually settles at 59.90 Hz (see the yellow trace in Fig. 19). In the GFL13 case, where only Gen 2 covers the 9 MW power deficit, the frequency drops from 59.96 Hz to as low as 59.71 Hz (0.25 Hz excursion) and eventually settles at 59.80 Hz (see the purple trace in Fig. 19), the lowest among all the cases analyzed.

C. VOLTAGE STABILITY

Another important aspect of system reliability is voltage stability. This class of stability analysis in transmission systems is directly linked to the availability of reactive power. In the base case, with all generators being SG, the generators respond when the system is subjected to 9 MW and 4.5 MVar load switching at bus 6 is such that all three generators adjust their reactive power generation. Gen 1 provides an additional 3 MVar, Gen 2 an additional 1.2 MVar, and Gen 3 an additional 1.9 MVar. As a result, voltage excursions

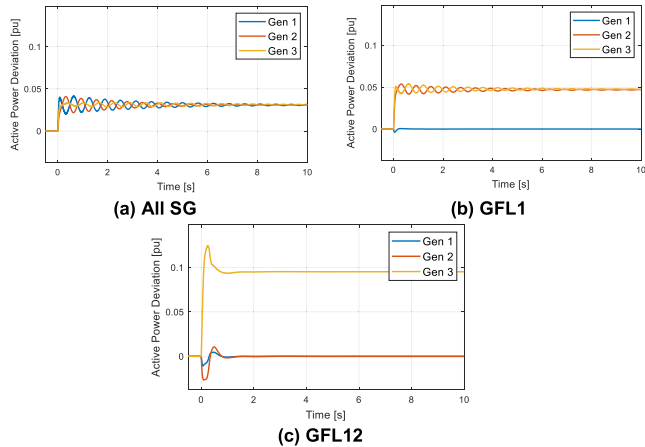


FIGURE 16. Active power response of the generators when the system is subjected to 9 MW load switching.

TABLE 1. Summary of generators' response following the change of loading conditions in bus 6 by 9 MW.

Case	Gen 1	Gen 2	Gen 3
All SG	3 MW	3 MW	3 MW
GFL1	0 MW	4.5 MW	4.5 MW
GFL2	4.5 MW	0 MW	4.5 MW
GFL3	4.5 MW	4.5 MW	0 MW
GFL12	0 MW	0 MW	9 MW
GFL13	0 MW	9 MW	0 MW
GFL23	9 MW	0 MW	0 MW

were arrested quickly and remained insignificant, as shown in Fig. 20(a). Subsequent cases were examined where SG was replaced with GFL to identify how the reactive power adjustment and voltage dynamics may change, and the results are presented in Fig. 20(b) and 20(c).

In the single IBR case, GFL1, GFL device does not contribute to adjusting its reactive power output and only retains its pre-disturbance output level. Since voltage is a local variable, the lack of adjustment of reactive power output by GFL can result in a voltage drop within the vicinity of GFL interconnection, which is a consistent observation in this case. Additionally, the reactive power is not transferable across the system. Therefore, the closer GFL is (in the electrical distance) to the disturbance's location, the more severe the voltage drop is. In this case, the switching takes place in bus 6, a terminating node for a transmission line to bus 4 (adjacent to bus 1), resulting in an exacerbated voltage drop which is attributed to the close proximity of GFL1 and switched load.

The observations in the double IBR case were similar to those in the single IBR case. The busbars near GFL experience voltage drop because of a lack of participation from GFL devices. In the GFL12 case, the only source of reactive power is the single remaining SG in bus 3. Considering the limitations associated with reactive power transfer, the voltage drops and the swings are more pronounced. Another point to note relates to the response from SG. Due to the lack of response from GFL, SG is forced to significantly adjust its reactive power output within a very short period to arrest the voltage declines.

TABLE 2. Description of the cases shown in Fig. 17.

Case	Gen 1	Gen 2	Gen 3
All SG	SG	SG	SG
GFL1	GFL	SG	SG
GFL2	SG	GFL	SG
GFL13	GFL	SG	GFL

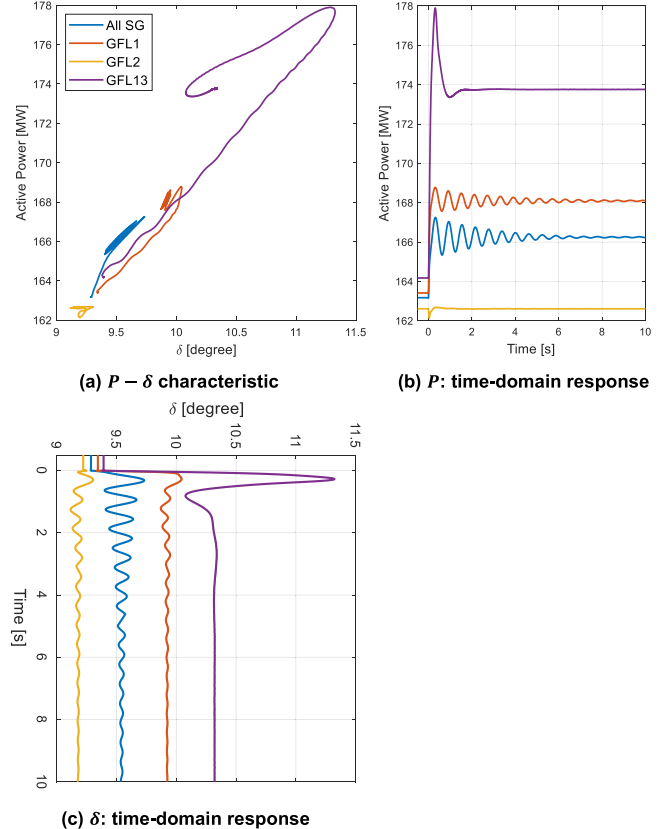


FIGURE 17. $P - \delta$ response of Gen 2 when the system is subjected to 9 MW load switching - All SG, GFL1, GFL2, and GFL13 cases.

Additionally, SG has to simultaneously adjust its active power output, as the prime function of a generator, to cover the active power deficit and arrest system frequency decline. This can significantly stress SG. In the case of a large load switching, SG's capability to adjust its reactive power output may be limited, depending on its operating power factor, which could trigger instability. This can be of special concern in the areas where the nature of the load is significantly reactive. Finally, similar to the single IBR case, the closer the GFL to the disturbance location, the more severe the voltage excursions, as seen in the GFL13 case. The results from other single cases were similar to GFL1 and the results from other double IBR cases were similar to that of GFL12 and, therefore, not shown.

Fig. 21 and Fig. 22 show the $P-V$ and $V-Q$ characteristics of the generator connected to bus 2 in four different cases, as described in Table 2. In the four cases considered here, the pre-disturbance voltage value is 1.025 p.u. The setting voltage value post-disturbance is approximately the same, 1.025 p.u.

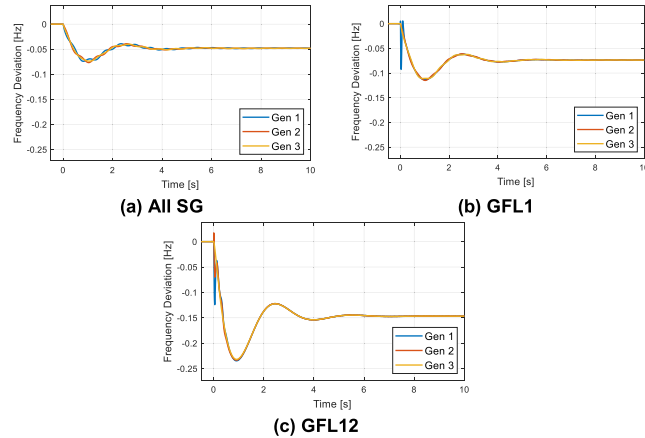


FIGURE 18. System frequency response when subjected to 9 MW load switching - GFL12, GFL13, and GFL12 cases.

for three cases and 1.023 p.u. for the GFL2 case. However, what distinguishes these cases are the active and reactive power and their relationship with transient low-voltage (TLV) and transient over-voltage (TOV).

In the All SG case, where all three generators are SG, the blue trace in Fig. 21 and Fig. 22, the output power of Gen 2 only moves by 3MW from 163 MW to 166 MW, but its transient oscillations peak at 167.2 MW (4.2 MW greater than the pre-disturbance value). Meanwhile, the reactive power moves by 1.4 MVar from 4.8 MVar to 6.2 MVar, with its transient peak at 6.8 MVar (2 MVar greater than the pre-disturbance value), resulting in the TLV and TOV of 1.023 and 1.025 p.u., respectively. This is a smooth power output adjustment.

In the GFL1 case, the red trace in Fig. 21 and Fig. 22, where only Gen 2 and Gen 3 equally participate in covering the 9 MW power deficit, Gen 2 adjusts its output by 4.5 MW from 163.5 MW to 168 MW with a transient oscillation peak at 168.7 MW (5.2 MW greater than the pre-disturbance value). Subsequently, output reactive power moves from 4.9 MVar to 8.7 MVar by 3.8 MVar with a peak transient at 9.7 MVar (4.8 MVar greater than the pre-disturbance value), and the resultant TLV and TOV are 1.020 and 1.026 p.u., respectively. The adjustment of power output and voltage dynamics are slightly exacerbated relative to the All SG case but still relatively smooth.

In the GFL2 case, where Gen 2 does not participate in covering the power deficit, the yellow trace in Fig. 21 and Fig. 22, Gen 2 power output experiences a minor temporary drop because of voltage transient and then quickly regains its pre-disturbance power and voltage set point. The TLV and TOV are 1.018 and 1.026 p.u., respectively.

In the GFL13 case, where only Gen 2 covers the 9 MW and 2.7 MVar power deficit, it adjusts its output by 9.5 MW from 164 MW to 173.5 MW with a transient peak at 177.8 MW (13.8 MW greater than the pre-disturbance output power), shown in purple trace in Fig. 21 and Fig. 22. Subsequently, the reactive power moves from 4.9 MVar to 17 MVar with a significant transient peak at 34.8 MVar (29.9 MVar greater than the pre-disturbance output power, six times the

TABLE 3. Summary of system frequency response following the change of loading conditions in bus 6 by 9 MW.

Case	Nadir Frequency [Hz]	Settling Frequency [Hz]	ROCOF [Hz/sec]
All SG	59.89	59.92	0.074
GFL1	59.85	59.89	0.113
GFL2	59.86	59.89	0.107
GFL3	59.85	59.89	0.109
GFL12	59.72	59.81	0.259
GFL13	59.70	59.80	0.288
GFL23	59.74	59.81	0.229

pre-disturbance output reactive power), and the TLV and TOV are 0.999 and 1.035 p.u., respectively. Such large transients can significantly stress SG, potentially trigger protective equipment.

A point to note here is that significant levels of IBR may force the trajectory of SGs to move so drastically that the frequent events that conventionally are understood and analyzed as small-signal stability problems (such as load switching or generation dispatch) could become large-signal stability problems.

The results for voltage dynamics from all cases considered here are summarized in Table 4. These results indicate a direct relationship between the percentage of SG in the system and TLV; the more SGs available, the higher the TLV. This is because SGs provide reactive power support to the grid during transient operations, including load switching. We could not make a definitive determination on a relationship between the replacement of IBR with SGs and TOV across the system (voltage values are local variables). Nonetheless, we identify the need for further investigation to better understand the sufficient headroom required for providing both active and reactive power support.

V. LARGE-SIGNAL STABILITY ANALYSIS AND DISCUSSION

This section presents the results from large-signal stability analysis and discusses the findings in the following order: (a) electric angle stability, (b) frequency response, and (c) voltage stability.

A. ELECTRIC ANGLE STABILITY

In the base case, with all generation units being SGs, when the system is subjected to a three-phase electric short circuit, the power output of generator connected to Bus 1 drops well below their normal operating points for the duration of the fault since the short-circuit takes place on Bus 1, as shown in Fig. 23(a). Once the fault is successfully cleared, because of the kinetic energy of the generator rotor that is accrued during the fault, the power oscillations emerge, and after a few swings, the transient energy gradually damps out. Eventually, the power output return to the pre-disturbance values. The response of a GFL during a fault is such that its power output rapidly drops, and if the fault is cleared successfully, it returns

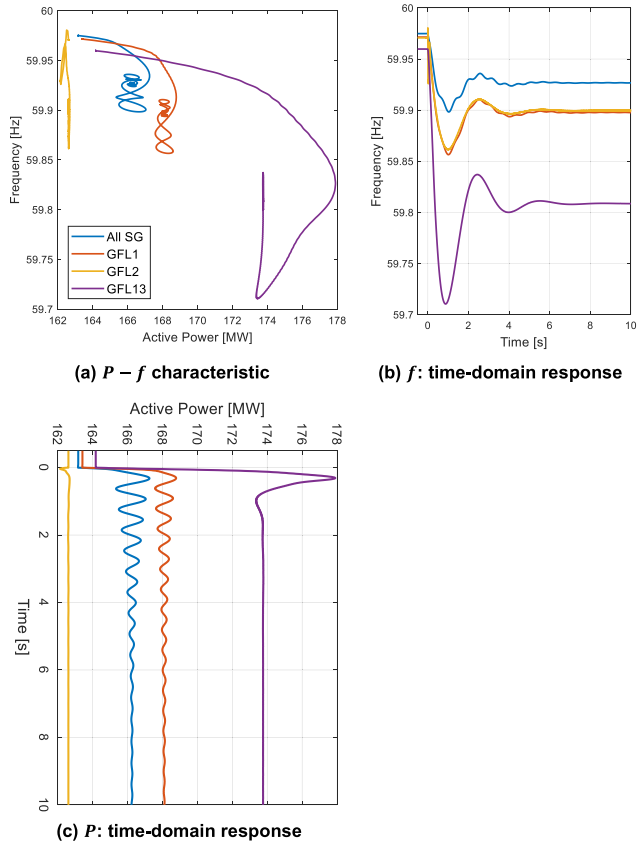


FIGURE 19. *P – f response of Gen 2 when the system is subjected to 9 MW load switching - All SG, GFL1, GFL2, and GFL13 cases.*

to the pre-disturbance value. To demonstrate the changes in system dynamics, all cases with IBR replacements were also subjected to a three-phase short circuit electrical fault on bus 1. First, the results for the single IBR case are presented in Fig. 23(b), and then the results from the double IBR case follow in Fig. 23(c).

In the single IBR case, GFL1, an exacerbated decrease in output power in GFL device is observed upon the inception of the fault. When the fault is cleared, GFL device offers a smooth return to the pre-disturbance output power value without any noticeable transient oscillations. SGs, however, experience exacerbated oscillations relative to the base case, including higher transient peak values following the clearance of the fault. This event can stress SGs and challenge the system's reliability. In the double IBR case, GFL12, similar to the single IBR cases, when the fault commences, the power output of the IBR devices drops but to a significantly greater extent. When the fault is cleared, the output returns to the pre-disturbance values. However, the recovery period for the IBR to recover becomes slightly longer than the single IBR cases. For SG devices, following the fault clearance, the transient peak significantly larger relative to the base case and single IBR cases. Nonetheless, the oscillations improve and damp out much faster. The results from other single cases were similar to that of GFL1 and the results from other double IBR cases were similar to that of GFL12 and, therefore, not

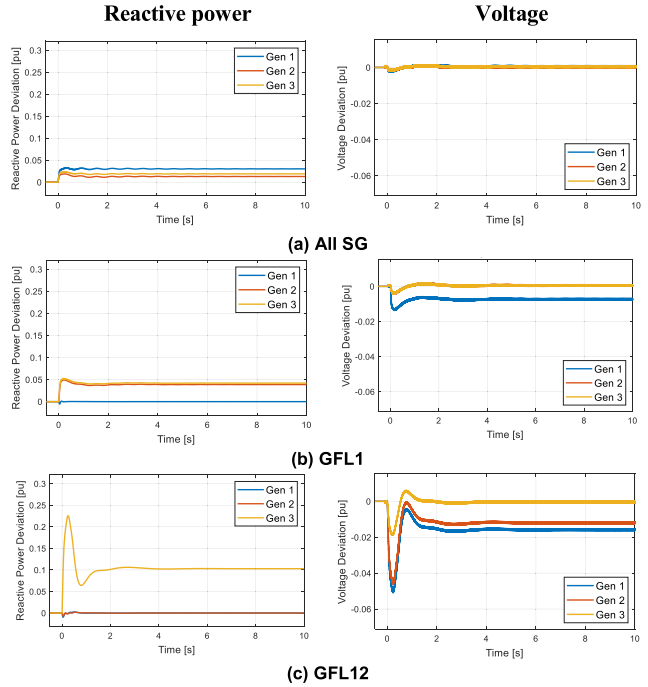


FIGURE 20. *Generator's reactive power adjustment and voltage dynamics when subjected to 9 MW load switching.*

shown. A summary of the generator responses—output active power—for all cases considered in this study is summarized in Table 5.

The results here show that the displacement of SGs and with IBRs can force the remaining SGs into more stressed transient operation with larger swings. This is mainly because when the fault is on, GFL effectively shuts down and does not provide any support to regain a stable operation. Subsequently, the impact of an SG disturbance is more severe, to the extent that the system may be unstable and become more susceptible to short-circuit electrical faults than a conventional power system with all SGs.

Fig. 24 shows the $P - \delta$ characteristics of the generator connected to bus 2 for four cases. Similar to the small-signal stability analysis, the selection of generator 2 and these four cases are an arbitrary choice and only for comparative demonstration purposes. The characteristics of other generators and other cases are similar and hence not shown. The cases indicated in this plot demonstrate four distinct operating conditions associated with the replacement of SGs with GFLs, as shown in Table 2.

In the All SG, GFL1, and GFL13 cases, shown in blue, red, and purple traces in Fig 24, where the Gen 2 is an SG, the power output drops, and the angle increases upon the fault inception. When the fault is successfully cleared, the power and angle return to their pre-disturbance values after dissipating the kinetic energy following transient oscillations. What distinguishes the three cases is the level of mechanical inertia and damping available in the system; All SG the highest (3 generators with inertia constant of $H = 4$), GFL1 medium (2 generators with inertia constant of $H = 4$),

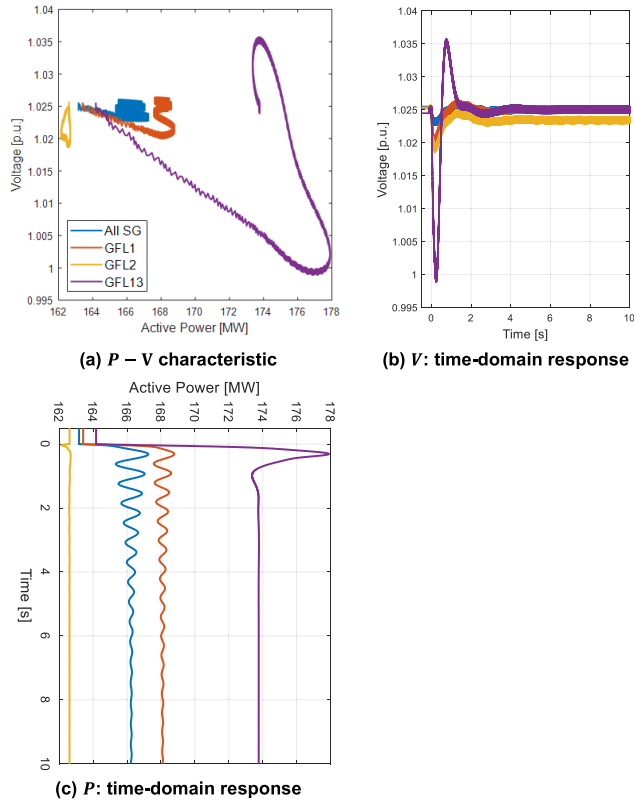


FIGURE 21. $P - V$ response of Gen 2 when the system is subjected to 9 MW load switching - All SG, GFL1, GFL2, and GFL13 cases.

TABLE 4. Summary of generators' voltage response following the change of loading conditions in bus 6 by 9 MW.

Case	TLV [p.u.]	TOV [p.u.]
All SG	1.022	1.041
GFL1	1.020	1.041
GFL2	1.018	1.041
GFL3	1.015	1.041
GFL12	0.980	1.041
GFL13	0.964	1.041
GFL23	0.988	1.046

and GFL13 the lowest (1 generator with inertia constant of $H = 4$). It is evident that reduced inertia and damping (which is provided by SG in the form of governor response) as a result of displacement of SG produces larger swings that take longer to damp out. In all three cases, the pre-disturbance active power output is roughly around 163 MW. During the transient operation, the active power peak in the All SG case reaches 173 MW (6% overshoot), while in the GFL1 case, it reaches 176 MW (8% overshoot). In GFL13, it is significantly exacerbated and reaches 191 MW (17% overshoot).

In the GFL2 case, where Gen 2 is a GFL, shown in yellow trace in Fig 24, immediately after the inception of the fault, the power output drops from 163 MW to 142 MW, and immediately after the fault clearance, it returns to its pre-disturbance set point. It should be noted that in all three

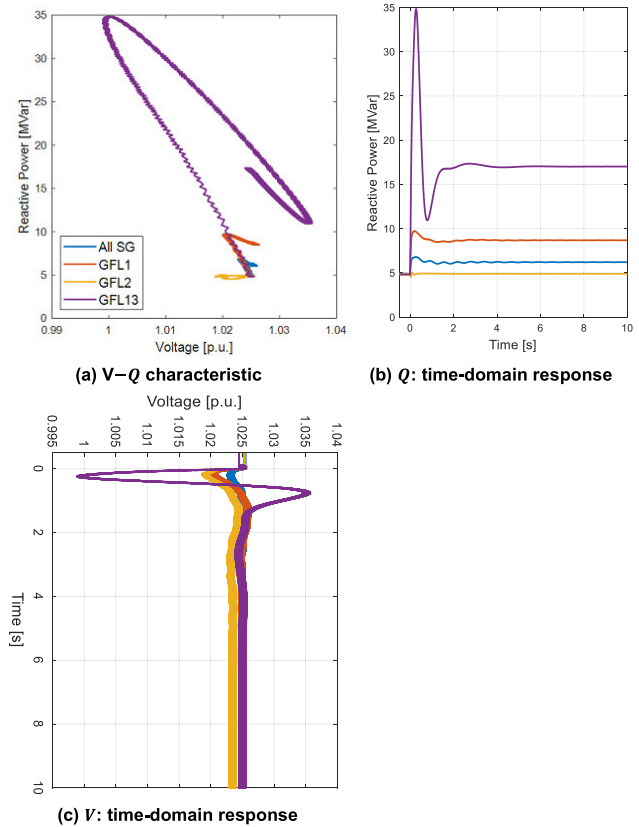


FIGURE 22. $V - Q$ response of Gen 2 when the system is subjected to 9 MW load switching - All SG, GFL1, GFL2, and GFL13 cases.

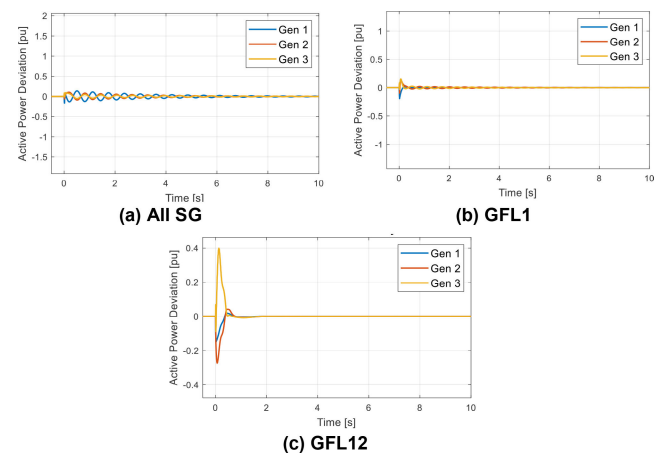


FIGURE 23. Active power response of the generators when the system is subjected to a three-phase short circuit electrical fault with a clearance time of 0.1 cycle.

cases where Gen 2 was an SG, the worst plunge of power was as low as 148 MW, in the GFL13 case, and in this case, where the Gen 2 is a GFL, it is lower and reaches as low as 142 MW.

The main point to observe here is the impact of displacement of SGs with GFL in faulted conditions and the adverse effect it can have on system transient operation; it stresses SG whilst GFL effectively shuts down during the transient operation.

TABLE 5. Summary of active power response of generators following a three-phase short circuit electrical fault on bus 1 with a clearance time of 0.1 cycle. Peak-to-peak transient power values are recorded during the post-fault [p.u.]

Case	Gen 1	Gen 2	Gen 3	Total Swing
All SG	0.29	0.15	0.10	0.54
GFL1	0.20	0.21	0.18	0.59
GFL2	0.36	0.21	0.19	0.76
GFL3	0.30	0.31	0.10	0.71
GFL12	0.15	0.31	0.47	0.93
GFL13	0.17	0.43	0.16	0.76
GFL23	0.64	0.52	0.26	1.42

B. FREQUENCY RESPONSE

The trace of frequency response in the base case with all generators being SG, system frequency response when subjected to a three-phase short-circuit electrical fault on bus 1 with a successful clearance at 0.1 cycle is displayed in Fig. 25(a). The frequency response for the subsequent cases where SGs were replaced with GFLs is presented in Fig. 25(b) and Fig. 25(c).

In the single IBR case, GFL1, when the fault occurs, the frequency measurement error by the PLL in GFL device immediately plunges while the frequency of SGs holds. This is a common challenge with GFL-IBR as observed in the Hawaiian power system and reported in [12]. The nadir frequency was below its value in the base case, and the ROCOF increased relative to the base case because of the reduced inertia. Following clearance of the fault, a frequency spike was observed. In the double IBR case, GFL12, similar to the single IBR case, when the fault takes place, the frequency of GFL devices immediately plunges. If the fault is successfully cleared within the CCT, then these devices regain their nominal frequency. However, the frequency in SGs holds closer to the nominal value when the fault is on because of the mechanical inertia and damping. The nadir frequency was lower, and ROCOF was higher in the double IBR case than in the base and single IBR case. The results from other single cases were similar to that of GFL1, and the results from other double IBR cases were similar to that of GFL12 were, and therefore not shown.

The results for frequency response from all cases considered are summarized in Table 4, excluding the transients caused by the PLL error. These results suggest a direct correlation between SGs and the system nadir frequency and ROCOF; the more SGs in operation, the closer to nominal the nadir frequency and lower the ROCOF. Fig. 26 shows the $P - \delta$ characteristics of the generator connected to busbar 2, described in Table 2.

In three cases here, Gen 2 is an SG, All SG, GFL1, and GFL13 cases, shown in blue, red, and purple traces in Fig 26, respectively. In all three cases, once the fault is cleared, the power output spikes, and following a few swings, it settles back at its pre-disturbance values. Nonetheless, the magnitude of the transient spike and subsequent oscillations are a function of available mechanical inertia in the system; the

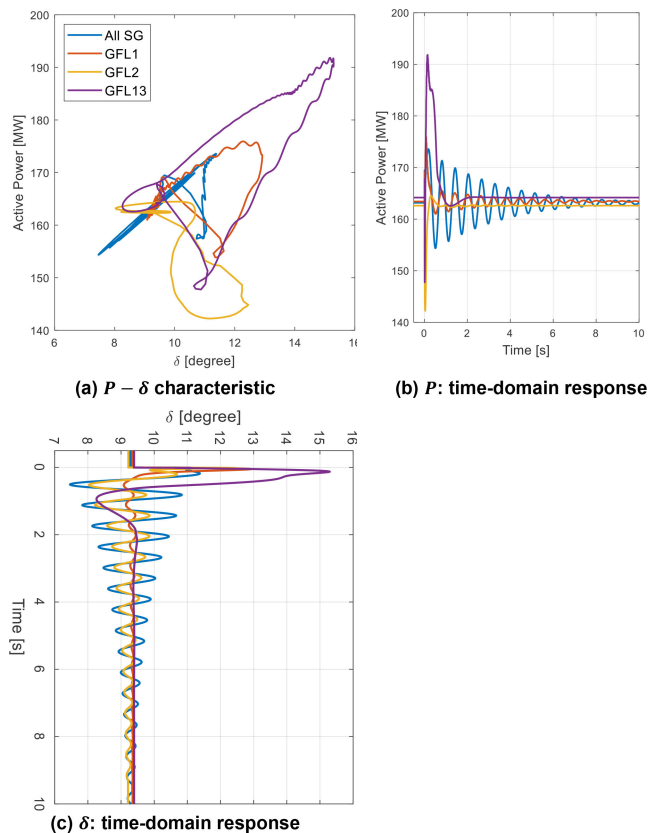


FIGURE 24. $P - \delta$ response of Gen 2 when the system is subjected to a three-phase short circuit electrical fault with a clearance time of 0.1 cycle - All SG, GFL1, GFL2, and GFL13 cases.

more SG online, the better the performance. Subsequently, the frequency response reflects the active power oscillations and, hence, the higher levels of SG online result in more mitigated frequency excursion. The oscillations and their ringing decay appear to be related to the availability of SGs; the higher the levels of SGs online in the system, the faster the ringing comes to a steady state.

In the GFL2 case where Gen 2 is a GFL, upon the fault inception, the power output plunges, and so does the frequency. However, once the fault is cleared, the power output immediately returns to the pre-disturbance value. The PLL error causes a momentary frequency spike, the yellow trace in Fig 26. This behavior could pose a potential challenge for protective elements.

C. VOLTAGE STABILITY

Voltage stability is directly a function of reactive power availability and generator ability to support reactive power. In the base case, with all generators being SG, the generator response when the system is subjected to a three-phase short-circuit electrical fault on bus 1 with a successful clearance at 0.1 cycle is such that all reactive power output of Gen 1, which is in the closest electric proximity of the fault, drops. In contrast, the reactive power output of the two other generators increases to provide support to the grid throughout

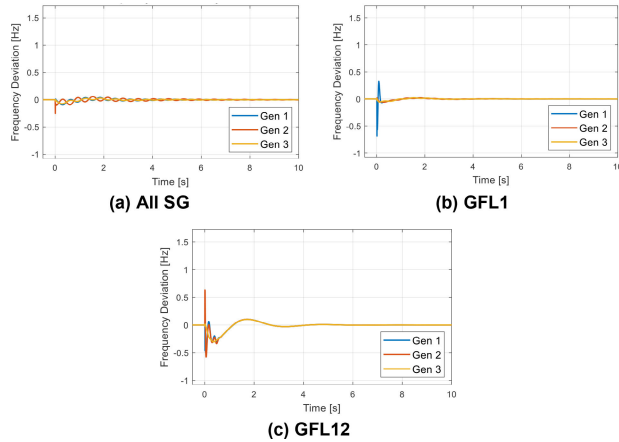


FIGURE 25. Frequency response of the generators when the system is subjected to a three-phase short circuit electrical fault with a clearance time of 0.1 cycle.

the transient operation, as shown in Fig. 27(a). As a result, the voltage drop at Gen 1 is more significant than in the two other generators. Subsequent cases examine the ramifications of replacing SGs with GFLs to identify potential voltage stability issues, and the results are presented in Fig. 27(b) and Fig. 27(c).

In the single IBR case, GFL1, GFL device does not provide any voltage support to the grid during the transient operation as opposed to SGs that supply a significant amount of reactive power when the fault is on, as shown in Fig. 27(b). It should be noted that some low voltage reactive power control approaches are possible, although not included in this analysis. This GFL behavior can be problematic from the perspective of voltage stability. The largest voltage drop was on Gen 1, which is closest to the fault. In the double IBR case, GFL12, consistent with the observations in the single IBR case, GFL devices do not provide voltage support to the grid during the transient operation. Their reactive power output does not increase when the fault is one, as shown in Fig. 27(c). On the other hand, SG provides additional support during the fault period. If SG reaches its reactive power limit, sustained voltage oscillations can lead to instability.

Fig. 28 and Fig. 29 show the $P-V$ and $V-Q$ characteristics of the generator connected to bus 2 for four different cases, as described in Table 2.

In the four cases considered here, the pre-disturbance voltage values are 1.025 p.u., and the setting voltage value post-disturbance is approximately the same. In the three cases where Gen 2 is an SG, All SG, GFL1, and GFL13, shown in blue, red, and purple traces in Fig. 28 and Fig. 29, when the fault is on, SG provides reactive support to the grid and the voltage excursions are well contained. However, the lower the levels of SGs in the system, the more severe the voltage swings. This is because of the lack of participation of GFL in the supply of reactive power, which forces SGs to supply a larger amount of reactive power in a short period. As a result, the swings become larger and can stress SGs and compromise the system stability limit.

TABLE 6. Summary of system frequency response following a three-phase short circuit electrical fault on bus 1 with a clearance time of 0.1 cycle.

Case	Pre-fault Frequency [Hz]	Nadir Frequency [Hz]	ROCOF [Hz/sec]
All SG	59.97	59.88	0.28
GFL1	59.97	59.91	0.54
GFL2	59.97	59.81	0.49
GFL3	59.97	59.81	0.47
GFL12	59.95	59.65	0.83
GFL13	59.95	59.62	0.52
GFL23	59.95	59.37	1.11

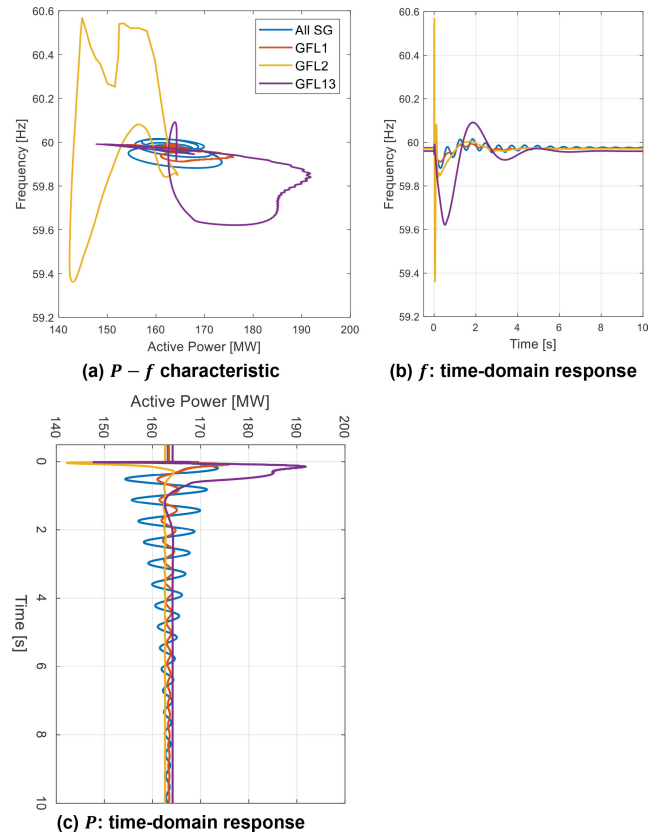


FIGURE 26. $P-f$ response of Gen 2 when the system is subjected to a three-phase short circuit electrical fault with a clearance time of 0.1 cycle - All SG, GFL1, GFL2, and GFL13 cases.

In the GFL2 case, shown in yellow trace in Fig. 28 and Fig. 29, where Gen 2 is a GFL and does not provide the grid with any support during the transient operation when the fault occurs, the voltage drops and, subsequently, active and reactive power drop. Once the fault is cleared, the power output returns to the pre-disturbance value.

The results for voltage dynamics from all cases considered here are summarized in Table 7, quantified by the lowest point of transient overvoltage (TOV) and the largest peak of transient low-voltage (TLV) observed, considering all generator buses.

The results in Table 7 indicate a direct relationship between the percentage of SGs being online and voltage swings, both

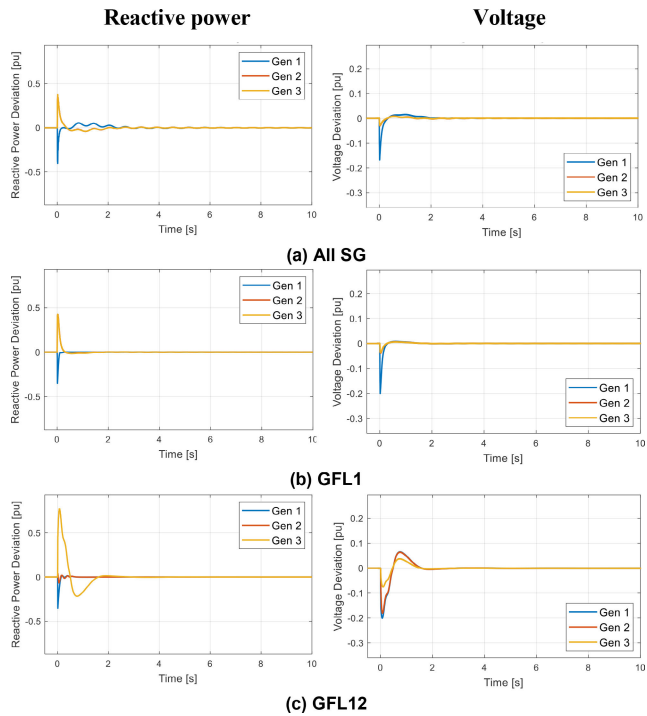


FIGURE 27. Response of the generators to adjustment of reactive power and voltage regulation when the system is subjected to a three-phase short circuit electrical fault with a clearance time of 0.1 cycle.

the TLV and the TOV; the more SG available, the smoother the voltage transients, resulting in higher TLVs and lower TOVs. This is because SGs provide reactive power support to the grid during transient operations, and GFL does not, as a baseline control approach. Operating a grid with low levels of SGs and high levels of GFL can challenge both the low-voltage protective elements and the overvoltage protective elements. It should be noted in All SG case, the TOV is slightly higher than the TOV in GFL1. This is because the voltage oscillations in All SG case are greater than in GFL1 case which is a result of an excited mode that only appears in All SG case. As a result, the peak of oscillations just happens to momentarily surpass the smoother response of the GFL1 case, though this is 0.007 p.u. difference which is significantly small. Effectively, the TOV for the two cases should be considered equal as the average value of the two cases is equal. The identification of the exact source of this excited voltage mode requires frequency domain analysis, which is beyond the scope of this paper.

D. IMPACT OF SYSTEM INERTIA

To understand the impact of inertia on transient stability, the base case and the subsequent scenarios involving GFL integration were examined for varying inertia levels. All the cases considered thus far assumed constant inertia of $H = 4\text{s}$ for each SG. For the sensitivity analysis, an arbitrary constant clearance time was chosen, and the cases were examined for a reduced inertia operation of $H = 2\text{s}$ and an increased inertia operation of $H = 6\text{s}$. The results presented here are for the frequency response, and the change of dynamics in other

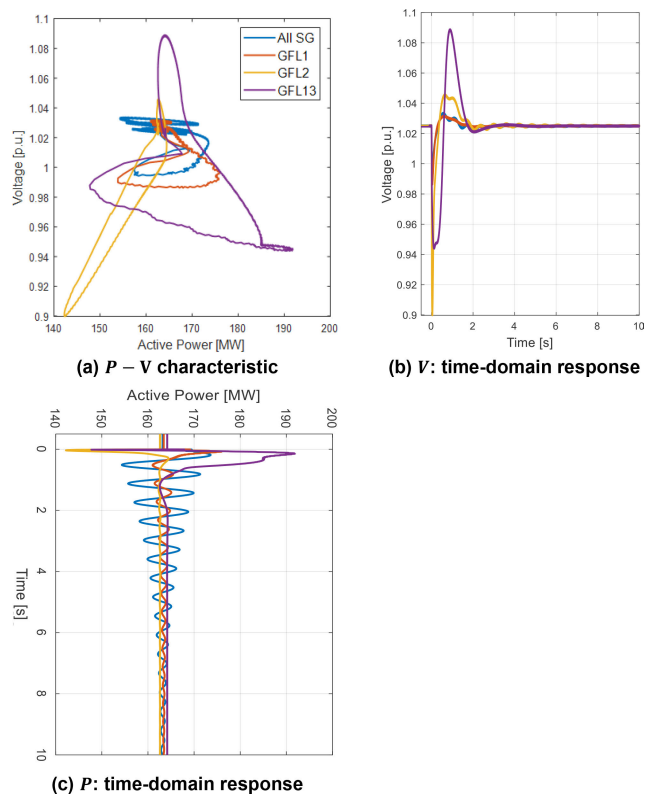


FIGURE 28. $P - V$ response of Gen 2 when the system is subjected to a three-phase short circuit electrical fault with a clearance time of 0.1 cycle - All SG, GFL1, GFL2, and GFL13 cases.

variables (e.g., power, voltage, etc.) are similar and, hence, not shown.

In the base case, with all generators being SG with identical inertia values, the system was subjected to a three-phase short circuit electrical fault, with a successful clearance within the CCT. The results, shown in Fig. 30(a), suggest that the increased mechanical inertia helps the system stabilize the oscillations faster and reduce the magnitude whilst the reduced mechanical inertia results in larger swings and oscillations. The deteriorated behavior is attributed to the absence of fast responding frequency-supporting devices to compensate for the impacts of reduced inertia. The frequency response for varying levels of inertia in the subsequent cases where SG was replaced with GFL is presented in Fig. 30(b) and Fig. 30(c).

In IBR cases, both the single IBR case and the double IBR case, it is evident that system dynamics were improved directly proportional to additional mechanical inertia. In low inertia operating conditions, the oscillations were more severe.

Most interesting observation was in the double IBR case, shown in Fig 30(c). In this case, the frequency response instability manifested itself in different behavior than what conventionally power system frequency instability is understood. In a conventional power system, frequency response instability is identified when the frequency trajectories in different areas of grid separate (because in one or more areas

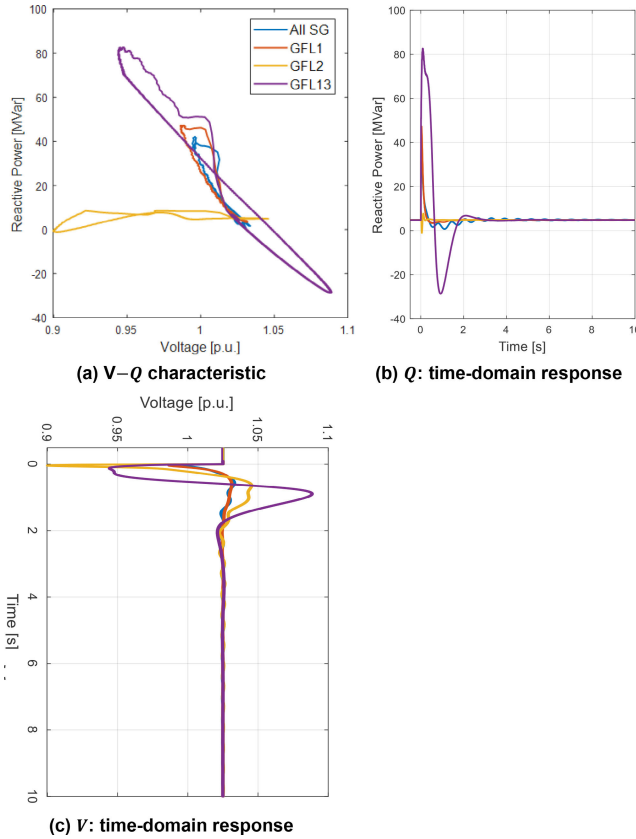


FIGURE 29. *V – Q response of Gen 2 when the system is subjected to a three-phase short circuit electrical fault with a clearance time of 0.1 cycle - All SG, GFL1, GFL2, and GFL13 cases.*

SG cannot supply enough mechanical power and frequency continues to decline) and force the formation of islands. Here, in the double IBR case, system frequency response instability was identified as spontaneous oscillations with seemingly nonhomogeneous oscillation periods and inconsistent magnitudes. We could not make a definite determination about the root cause of this phenomenon, but our understanding suggests that these chaotic motions could be linked to the interaction of PLLs. Moreover, we speculated the different frequency response observed here is because there are GFL devices injecting power into the system objectively without any active controller that adjusts its operation subject to grid conditions. Whereas in a traditional power system, with all grid-forming type SGs, instability would just manifest as separation and, therefore, GFL are not susceptible to the same angle analysis as the grid-forming SG devices.

Overall, in all three cases, the additional mechanical inertia helped to stabilize the unstable cases; the yellow traces are in Fig. 30.

E. SYSTEM STABILITY LIMIT

The system CCT can measure power system transient stability. As a reminder, the CCT is the longest period of fault persistence, leading to the system regaining a stable operation following the fault clearance. The CCT is generally

TABLE 7. *Summary of generators' voltage response following a three-phase short circuit electrical fault on bus 1 with a clearance time of 0.1 cycle.*

Case	TLV [p.u.]	TOV [p.u.]
All SG	0.871	1.055
GFL1	0.839	1.048
GFL2	0.854	1.060
GFL3	0.855	1.060
GFL12	0.840	1.106
GFL13	0.846	1.143
GFL23	0.704	1.281

TABLE 8. *Summary of system stability limit following a three-phase short circuit electrical fault on bus 6.*

Case	Stability Limit [cycles]
All SG	147
GFL1	16
GFL2	30
GFL3	17.5
GFL12	0.5
GFL13	0.1
GFL23	0.0

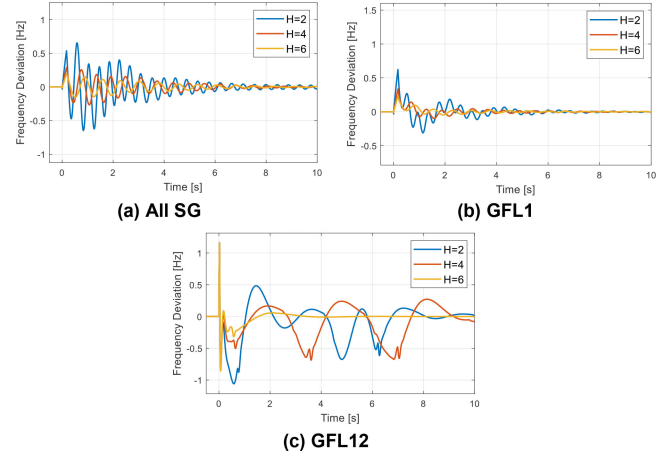


FIGURE 30. *System frequency response to a three-phase short circuit electrical fault for varying levels of inertia at a boundary condition – All SG and single IBR cases at 10 cycles clearance; double IBR cases at 1 cycle clearance.*

considered a system stability limit. A summary of the system stability limit for the cases considered is presented in Table 8.

The results here suggest that the replacement of SG with GFL IBR can significantly reduce the system stability limit. In this case study, GFL installations reduced the stability by an order of magnitude. This shows the additional mechanical inertia present in the system increases the stability limit hence improving the system transient stability. The deterioration of transient stability is mainly because of the lack of fast responding devices (e.g., GFM inverters) to mitigate the adverse impacts of the displacement of SGs.

VI. FINDINGS AND CONCLUSION

This paper addresses the stability and reliability challenges pertinent to the integration of GFL interfaced IBRs, with an

emphasis on the characterization of the dynamic interactions between SG and GFL at the system level. It develops a guideline to explain the underlying interrelated dynamics of electric angle, frequency, and voltage with high shares of IBR as well as the impacts that system inertia can have on the system stability. Industry-grade EMT simulations demonstrate the concepts presented in this guideline and all the models have been made available to the public at no cost.

It studies both small-signal and large-signal stability problems. Small-signal stability is concerned with the system behavior and convergence when subjected to an external disturbance that does not result in topological or configuration change, e.g., load switching or changes in generation dispatch. Large-signal stability is concerned with the system behavior when subjected to an external disturbance that results in topological or configuration changes, e.g., an electrical fault or a loss of components (e.g., lines or generators).

The analyses provided in this paper offer valuable insights into the industry's current state of integrating VRE and the underlying phenomena that could challenge power grid reliability and stability. This paper sets a basis for further exploration of power system dynamics with high shares of GFL-IBRs and the development of more advanced control strategies to manage such power systems. Additional research is essential to better understand the interactions between and the parallel operation of the grid-following and the grid-forming technologies.

A. SMALL-SIGNAL STABILITY

Our findings suggest that replacing SGs with GFL-IBRs can significantly reduce the small-signal stability of a power grid. This is mainly because GFL does not participate in system power balance regulation, which can stress the remaining SGs. SG units then are forced to offer larger changes in their output, which inherently results in larger swings to cover the deficit, making it closer to the critical power output. As a result, significant levels of IBR may force the trajectory of SGs to move so drastically that the frequent events that conventionally are understood and analyzed as a small-signal stability problem (e.g., load switching) could become large-signal stability problems.

When a power grid is subjected to a small disturbance, the more available headroom reserve in operation, the smaller the frequency deviations. Our findings indicate that with the displacement of SG, the inability of GFL to adjust their output to compensate for power imbalances effectively reduces the system's overall headroom reserve. As a result, the effective system frequency-droop gain increases, resulting in deteriorated frequency response.

This study also finds that replacing SG with GFL can adversely affect the system's voltage stability. GFL does not provide any voltage support to the grid; thus, SG is forced to significantly adjust its reactive power output within a very short period to arrest the voltage declines. Additionally, SG has to simultaneously adjust its active power output, as the prime function of a generator, to cover the active power deficit

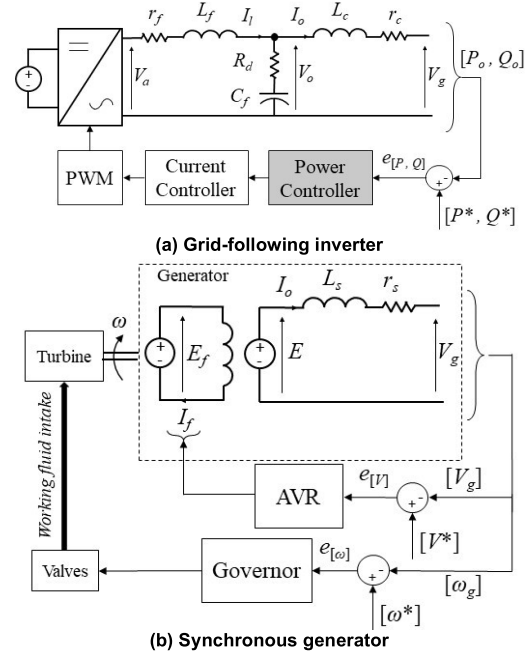


FIGURE 31. High-level circuit and control diagram for GFL and SG.

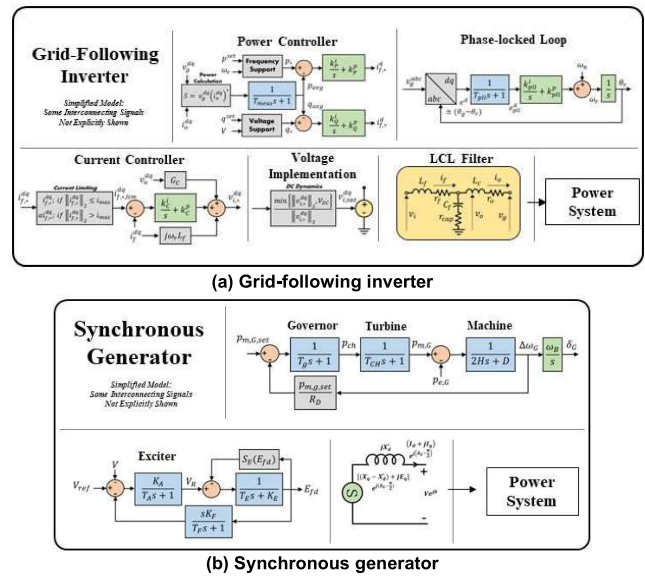


FIGURE 32. Detailed control diagram for GFL and SG.

and arrest system frequency decline. This can significantly stress SG and force instability. Further study is recommended to better understand the headroom reserve required for both active and reactive power support.

B. LARGE-SIGNAL STABILITY

Our findings suggest that the displacement of SGs, by GFL type IBRs, can force the remaining SGs into more stressed transient operations with larger swings. This is mainly because when the fault is on, GFL effectively shuts down (similar to a momentary cessation). Subsequently, an SG's effective fault is more severe, to the extent that the system

TABLE 9. Transmission lines parameters.

From node	To node	<i>r</i>	<i>x</i>	<i>b</i>
1	4	0	0.0576	0
4	6	0.017	0.092	0.158
9	6	0.039	0.17	0.358
3	9	0	0.0586	0
8	9	0.0119	0.1008	0.209
7	8	0.0085	0.072	0.149
7	2	0	0.0625	0
5	7	0.032	0.161	0.306
5	4	0.01	0.085	0.176

TABLE 10. Generators dispatch.

Generator	Node Connection	P (MW)	Q (MVar)
1	1	71.96	27.6
2	2	163.2	4.9
3	3	85.3	-11.4

TABLE 11. Load values.

Load	Node Connection	P (MW)	Q (MVar)
1	5	125	50
2	6	90	30
3	8	100	35

will be inherently unstable and susceptible to any short-circuit electrical fault.

Our results further reveal that the replacement of SGs with GFLs can result in larger system frequency oscillations and deviation when subjected to a contingency, e.g., short-circuit fault or loss of component(s), and the reason for it is twofold. First, the reduced effective system inertia (because of the displacement of SGs) results in larger frequency oscillations and excursion, for example during the fault or immediately after the loss of component(s). Second, the aggregate system frequency droop value increases, compromising the system ability to damp out frequency oscillations and restore the system-wide frequency.

It was also found out that the lack of participation of GFLs in supplying reactive power during faults can force SGs to supply a larger amount of reactive power in a short period. As a result, the power and voltage swings increase and can stress SGs and compromise the system stability limit.

Our results establish that replacing SGs with GFLs can significantly reduce the system stability limit; in the case study used here, the limit described by the critical clearing time was reduced by orders of magnitude, which is significant for system reliability. Additional mechanical inertia can improve system transient stability. We recommend that the chaotic motions observed in the system frequency response during very low inertia operating conditions require further investigation.

APPENDIX I

The control and circuit diagrams of SG and GFL inverter are shown in Figs. 31 and 32. The open-source computer models

TABLE 12. Power flow.

Node	Voltage (p.u.)	Angle (degree)
1	1.00	0
2	1.025	10
3	1.025	5
4	1.02	-2
5	1.00	-4.3
6	1.01	-4
7	1.02	4
8	1.01	1.3
9	1.03	2

TABLE 13. Synchronous generator parameters.

Component	Parameter	Value [p.u.]
Machine	Nominal Voltage (kV)	9.52
	Nominal Voltage (kA)	7.00
	Inertia	4
AGC	Time Step	2
	Gain	0.1
Governor	Droop Gain	0.05
	Time Constant	0.5

TABLE 14. Grid-following inverter parameters.

Component	Parameter	Value [p.u.]
Current Limiting	Q Current Limiting	-1.0/1.0
	P Current Limiting	0.0/1.0
Physical Components	Filter Inductor	0.009
	Filter Resistance	0.016
	Coupling Inductor	0.0017
	Coupling Resistance	0.003
	Filter Capacitance	2.55
	Capacitance Resistance	0.0005
	PLL Filter	500
PLL	Measurement Filter	50
	Integral Gain	415
	Proportional Gain	52
	P Integral Gain	21
Power Controller	P Proportional Gain	2.1
	Q Integral Gain	20.8
	Q Proportional Gain	2.08
	Integral Gain	0.70
Current Controller	Proportional Gain	0.38
	Feedforward Gain	1.0

used in this study, available on NREL Github [59], have been built based on these circuit and control structures.

APPENDIX II

The parameters of lines and generators used in this study.

ACKNOWLEDGMENT

The views expressed in the article do not necessarily represent the views of the DOE or the U.S. Government. The U.S. Government retains and the publisher, by accepting the article for publication, acknowledges that the U.S. Government retains a nonexclusive, paid-up, irrevocable, worldwide license to publish or reproduce the published form of this work, or allow others to do so, for U.S.

REFERENCES

- [1] *Levelized Cost of Energy and Levelized Cost of Storage 2020*, Lazard Consultant, Hamilton, Bermuda, 2020. Accessed: Feb. 8, 2020.
- [2] N. Chestney, "Record 260 GW of new renewable energy capacity added in 2020: Research," Reuters, 2020. [Online]. Available: <https://www.reuters.com/article/us-climate-change-renewables/record-260-gw-of-new-renewable-energy-capacity-added-in-2020-research-idUSKBN2BT0UL>
- [3] *Renewable Energy Market Update*, IEA-Int. Energy Agency, Paris, France, 2021.
- [4] *Renewable Energy Market Update 2021—Outlook for 2021*, IEA-Int. Energy Agency, Paris, France, 2022.
- [5] O. Waszczuk, "Dynamic behavior of a class of photovoltaic power systems," *IEEE Trans. Power App. Syst.*, vol. PAS-102, no. 9, pp. 3031–3037, Sep. 1983.
- [6] T. S. Key, "Evaluation of grid-connected inverter power systems: The utility interface," *IEEE Trans. Ind. Appl.*, vol. IA-20, no. 4, pp. 735–741, Jul. 1984.
- [7] K. C. Kalaitzakis and G. J. Vachtsevanos, "On the control and stability of grid connected photovoltaic sources," *IEEE Trans. Energy Convers.*, vol. EC-2, no. 4, pp. 556–562, Dec. 1987.
- [8] O. Waszczuk, "Modeling and dynamic performance of a line-commutated photovoltaic inverter system," *IEEE Power Eng. Rev.*, vol. 9, no. 9, pp. 35–36, Sep. 1989.
- [9] G. Kern, R. Bonn, J. Ginn, and S. Gonzalez, "Results of Sandia national laboratories grid-tied inverter testing," Sandia Nat. Labs., Albuquerque, NM, USA, Tech. Rep. SAND-98-1540C, 1998.
- [10] I. H. Hwang, K. S. Ahn, H. C. Lim, and S. S. Kim, "Design, development and performance of a 50 kW grid connected PV system with three phase current-controlled inverter," in *Proc. Conf. Rec. 28th IEEE Photovoltaic Spec. Conf.*, Sep. 2000, pp. 1664–1667.
- [11] J. G. Slootweg, H. Polinder, and W. L. Kling, "Dynamic modelling of a wind turbine with doubly fed induction generator," in *Proc. Power Eng. Soc. Summer Meeting*, vol. 1. Jul. 2001, pp. 644–649.
- [12] P. S. Georgilakis, "Technical challenges associated with the integration of wind power into power systems," *Renew. Sustain. Energy Rev.*, vol. 12, no. 3, pp. 852–863, 2008.
- [13] S. Jain and V. Agarwal, "A single-stage grid connected inverter topology for solar PV systems with maximum power point tracking," *IEEE Trans. Power Electron.*, vol. 22, no. 5, pp. 1928–1940, Sep. 2007.
- [14] G. Velasco, F. Guinjoan, R. Pique, and J. J. Negroni, "Sizing factor considerations for grid-connected PV systems based on a central inverter configuration," in *Proc. 32nd Annu. Conf. IEEE Ind. Electron.*, Nov. 2006, pp. 2718–2722.
- [15] Y. Chen and K. Smedley, "Three-phase boost-type grid-connected inverter," *IEEE Trans. Power Electron.*, vol. 23, no. 5, pp. 2301–2309, Sep. 2008.
- [16] B. S. Prasad, S. Jain, and V. Agarwal, "Universal single-stage grid-connected inverter," *IEEE Trans. Energy Convers.*, vol. 23, no. 1, pp. 128–137, Mar. 2008.
- [17] B. Crowhurst, E. F. El-Saadany, L. E. Chaar, and L. A. Lamont, "Single-phase grid-tie inverter control using DQ transform for active and reactive load power compensation," in *Proc. IEEE Int. Conf. Power Energy*, Nov. 2010, pp. 489–494.
- [18] E. H. Camm and S. E. Williams, "Solar power plant design and interconnection," in *Proc. IEEE Power Energy Soc. Gen. Meeting*, Jul. 2011, pp. 1–3.
- [19] P. Mackin, R. Daschmans, B. Williams, B. Haney, R. Hunt, J. Ellis, and J. H. Eto, "Dynamic simulation study of the frequency response of the western interconnection with increased wind generation," in *Proc. 46th Hawaii Int. Conf. Syst. Sci.*, 2013, pp. 2222–2229.
- [20] N. Miller, M. Shao, S. Pajic, and R. D'Aquila, "Eastern frequency response study," Nat. Renew. Energy Lab. (NREL), Golden, CO, USA, Tech. Rep. NREL/TP-6A20-64472, 2013.
- [21] A. Ulbig, T. S. Borsche, and G. Andersson, "Impact of low rotational inertia on power system stability and operation," *IFAC Proc. Volumes*, vol. 47, no. 3, pp. 7290–7297, 2014.
- [22] G. Kou, P. Markham, S. Hadley, T. King, and Y. Liu, "Impact of governor deadband on frequency response of the U.S. Eastern interconnection," *IEEE Trans. Smart Grid*, vol. 7, no. 3, pp. 1368–1377, May 2016.
- [23] N. W. Miller, M. Shao, R. D'Aquila, S. Pajic, and K. Clark, "Frequency response of the U.S. Eastern interconnection under conditions of high wind and solar generation," in *Proc. 7th Annu. IEEE Green Technol. Conf.*, Apr. 2015, pp. 21–28.
- [24] S. You, Y. Liu, X. Zhang, Y. Su, L. Wu, Y. Liu, and S. W. Hadley, "Impact of high PV penetration on U.S. Eastern interconnection frequency response," in *Proc. IEEE Power Energy Soc. Gen. Meeting*, Jul. 2017, pp. 1–5.
- [25] S. You, G. Kou, Y. Liu, X. Zhang, Y. Cui, M. J. Till, W. Yao, and Y. Liu, "Impact of high PV penetration on the inter-area oscillations in the U.S. Eastern interconnection," *IEEE Access*, vol. 5, pp. 4361–4369, 2017.
- [26] J. Tan, Y. Zhang, S. You, Y. Liu, and Y. Liu, "Frequency response study of U.S. Western interconnection under extra-high photovoltaic generation penetrations," in *Proc. IEEE Power Energy Soc. Gen. Meeting (PESGM)*, Aug. 2018, pp. 1–5.
- [27] F. Milano, F. Dörfler, G. Hug, D. J. Hill, and G. Verbić, "Foundations and challenges of low-inertia systems," in *Proc. Power Syst. Comput. Conf. (PSCC)*, 2018, pp. 1–25.
- [28] J. Eto, "CERTS microgrid laboratory test bed," Lawrence Berkeley Nat. Lab., Tech. Rep., 2009.
- [29] R. H. Lasseter, J. H. Eto, B. Schenkman, J. Stevens, H. Vollkommer, D. Klapp, E. Linton, H. Hurtado, and J. Roy, "CERTS microgrid laboratory test bed," *IEEE Trans. Power Del.*, vol. 26, no. 1, pp. 325–332, Jan. 2011.
- [30] D. Pattabiraman, R. H. Lasseter, and T. M. Jahns, "Comparison of grid following and grid forming control for a high inverter penetration power system," in *Proc. IEEE Power Energy Soc. Gen. Meeting (PESGM)*, Aug. 2018, pp. 1–5.
- [31] M. G. Taul, X. Wang, P. Davari, and F. Blaabjerg, "An efficient reduced-order model for studying synchronization stability of grid-following converters during grid faults," in *Proc. 20th Workshop Control Modeling Power Electron. (COMPEL)*, Jun. 2019, pp. 1–7.
- [32] B. J. Pierre, H. N. V. Pico, R. T. Elliott, J. Flicker, Y. Lin, B. B. Johnson, J. H. Eto, R. H. Lasseter, and A. Ellis, "Bulk power system dynamics with varying levels of synchronous generators and grid-forming power inverters," in *Proc. IEEE 46th Photovoltaic Spec. Conf. (PVSC)*, Jun. 2019, pp. 880–886.
- [33] M.-S. Debry, G. Denis, and T. Prevost, "Characterization of the grid-forming function of a power source based on its external frequency smoothing capability," in *Proc. IEEE Milan PowerTech*, Jun. 2019, pp. 1–6.
- [34] B. K. Poolla, D. Groß, and F. Dörfler, "Placement and implementation of grid-forming and grid-following virtual inertia and fast frequency response," *IEEE Trans. Power Syst.*, vol. 34, no. 4, pp. 3035–3046, Jul. 2019.
- [35] D. Gross and F. Dorfler, "Projected grid-forming control for current-limiting of power converters," in *Proc. 57th Annu. Allerton Conf. Commun., Control, Comput. (Allerton)*, Sep. 2019, pp. 326–333.
- [36] S. F. Zarei, H. Mokhtari, M. A. Ghasemi, S. Peyghami, P. Davari, and F. Blaabjerg, "Control of grid-following inverters under unbalanced grid conditions," *IEEE Trans. Energy Convers.*, vol. 35, no. 1, pp. 184–192, Mar. 2020.
- [37] A. Sajadi, R. W. Kenyon, M. Bossart, and B.-M. Hodge, "Dynamic interaction of grid-forming and grid-following inverters with synchronous generators in hybrid power plants," in *Proc. IEEE Kansas Power Energy Conf. (KPEC)*, Apr. 2021, pp. 1–6.
- [38] R. W. Kenyon, A. Hoke, J. Tan, and B.-M. Hodge, "Gridfollowing inverters and synchronous condensers: A grid-forming pair?" in *Proc. Clemson Univ. Power Syst. Conf. (PSC)*, 2020, pp. 1–7.
- [39] N.-B. Lai, A. Tarraso, G. N. Baltas, L. V. M. Arevalo, and P. Rodriguez, "External inertia emulation controller for grid-following power converter," *IEEE Trans. Ind. Appl.*, vol. 57, no. 6, pp. 6568–6576, Nov. 2021.
- [40] B. Pawar, E. Batzelis, S. Chakrabarti, and B. Pal, "Grid-forming control for solar PV systems with power reserves," *IEEE Trans. Sustain. Energy*, vol. 12, no. 4, pp. 1947–1959, Oct. 2021.
- [41] Y. Jiang, A. Bernstein, P. Vorobev, and E. Mallada, "Grid-forming frequency shaping control for low-inertia power systems," in *Proc. Amer. Control Conf. (ACC)*, May 2021, pp. 4184–4189.
- [42] C. Yang, L. Huang, H. Xin, and P. Ju, "Placing grid-forming converters to enhance small signal stability of PLL-integrated power systems," *IEEE Trans. Power Syst.*, vol. 36, no. 4, pp. 3563–3573, Jul. 2021.
- [43] *Reliability Guideline: BPS-Connected Inverter-Based Resource Performance*, North America Electric Reliability Corporation (NERC), Atlanta, GA, USA, 2018.
- [44] D. G. Photovoltaics and E. Storage, *IEEE Standard Conformance Test Procedures for Equipment Interconnecting Distributed Energy Resources With Electric Power Systems and Associated Interfaces*, Standard 1547.1-2020, 2020.
- [45] T. S. Basso and R. DeBlasio, "IEEE 1547 series of standards: Interconnection issues," *IEEE Trans. Power Electron.*, vol. 19, no. 5, pp. 1159–1162, Sep. 2004.

- [46] R. Guttrumson and M. Behnke, "Momentary cessation: Improving dynamic performance and modeling of utility-scale inverter based resources during grid disturbances," Sandia Nat. Lab. (SNL-NM), Albuquerque, NM, USA, Tech. Rep. SAN D2020-0266, 2020.
- [47] A. Lorenzo-Bonache, A. Honrubia-Escribano, J. Fortmann, and E. Gómez-Lázaro, "Generic type 3 WT models: Comparison between IEC and WECC approaches," *IET Renew. Power Gener.*, vol. 13, no. 7, pp. 1168–1178, May 2019.
- [48] A. Lorenzo-Bonache, A. Honrubia-Escribano, F. Jimenez-Buendia, and E. Gomez-Lazaro, "Field validation of generic type 4 wind turbine models based on IEC and WECC guidelines," *IEEE Trans. Energy Convers.*, vol. 34, no. 2, pp. 933–941, Jun. 2019.
- [49] G. Lammerl, L. D. P. Ospina, P. Pourbeik, D. Fetzer, and M. Braun, "Implementation and validation of WECC generic photovoltaic system models in DIgSILENT PowerFactory," in *Proc. IEEE Power Energy Soc. Gen. Meeting (PESGM)*, Jul. 2016, pp. 1–5.
- [50] A. Ellis, E. Muljadi, J. Sanchez-Gasca, and Y. Kazachkov, "Generic models for simulation of wind power plants in bulk system planning studies," in *Proc. IEEE Power Energy Soc. Gen. Meeting*, Jul. 2011, pp. 1–8.
- [51] R. T. Elliott, A. Ellis, P. Pourbeik, J. J. Sanchez-Gasca, J. Senthil, and J. Weber, "Generic photovoltaic system models for WECC—A status report," in *Proc. IEEE Power Energy Soc. Gen. Meeting*, Jul. 2015, pp. 1–5.
- [52] *1,200 MW Fault Induced Solar Photovoltaic Resource Interruption Disturbance Report*, North America Electric Reliability Corporation (NERC), Atlanta, GA, USA, 2016.
- [53] *October 9, 2017 Canyon 2 Fire Disturbance Report*, North America Electric Reliability Corporation (NERC), Atlanta, GA, USA, 2016.
- [54] J. Nerc and T. R. Staff, "April and May 2018 fault induced solar photovoltaic resource interruption disturbances report: Southern California events: April 20, 2018 and May 11, 2018," NERC, Atlanta, GA, USA, Tech. Rep., 2019. [Online]. Available: https://www.nerc.com/pa/frm/ea/April_May_2018_Fault_Induced_Solar_PV_Resource_Int/April_May_2018_Solar_PV_Disturbance_Report.pdf
- [55] J. Nerc and T. R. Staff, "San Fernando disturbance, Southern California event: July 7, 2020," NERC, Atlanta, GA, USA, Tech. Rep., 2020. [Online]. Available: https://www.nerc.com/pa/rrm/ea/Documents/Odessa_Disturbance_Report.pdf
- [56] J. Nerc and T. R. Staff, "Odessa disturbance Texas events: May 9, 2021 and June 26, 2021," NERC, Atlanta, GA, USA, Tech. Rep., 2021.
- [57] J. Machowski, J. Bialek, and J. Bumby, *Power System Dynamics: Stability and Control*. Hoboken, NJ, USA: Wiley, 2008.
- [58] T. van Cutsem and C. Vournas, *Voltage Stability of Electric Power Systems*. Cham, Switzerland: Springer, 1998.
- [59] R. W. Kenyon. (Nov. 2020). *PyPSCAD*. [Online]. Available: <https://github.com/NREL/PyPSCAD>
- [60] R. W. Kenyon, A. Sajadi, A. Hoke, and B.-M. Hodge, "Open-source PSCAD grid-following and grid-forming inverters and a benchmark for zero-inertia power system simulations," in *Proc. IEEE Kansas Power Energy Conf. (KPEC)*, Apr. 2021, pp. 1–6.
- [61] A. Sajadi, R. W. Kenyon, and B.-M. Hodge, "Synchronization in electric power networks with inherent heterogeneity up to 100% inverter-based renewable generation," *Nature Commun.*, vol. 13, no. 1, pp. 1–12, May 2022.
- [62] R. W. Kenyon, B. Wang, A. Hoke, J. Tan, C. Antonio, and B.-M. Hodge, "Validation of Maui PSCAD model: Motivation, methodology, and lessons learned," in *Proc. 52nd North Amer. Power Symp. (NAPS)*, Apr. 2021, pp. 1–6.
- [63] R. D. Zimmerman, C. E. Murillo-Sánchez, and R. J. Thomas, "MATPOWER: Steady-state operations, planning, and analysis tools for power systems research and education," *IEEE Trans. Power Syst.*, vol. 26, no. 1, pp. 12–19, Feb. 2011.



JO ANN RAÑOLA (Member, IEEE) is a Technical Leader with the Electric Power Research Institute (EPRI). She has more than 15 years of combined experience in analyzing various models—capacity expansion models, production cost models, resource adequacy, and financial—and developing business development cases across countries, such as the USA, Australia, the Philippines, Singapore, and Vietnam. Her research interests include grid-integration studies and resource adequacy initiatives.



RICK WALLACE KENYON (Member, IEEE) received the Ph.D. degree from the University of Colorado at Boulder, USA. He is a Senior Mathematical Modeler with encoord, where he studies hybrid simulation platforms for assessing the dynamic security of power systems with large shares of renewable resources. His main research interest includes the potential for nonlinear frequency control with grid-forming control, to enable the decarbonization of the grids.



BRI-MATHIAS HODGE (Senior Member, IEEE) received the B.S. degree from Carnegie Mellon University, the M.S. degree from Abo Akademi University, and the Ph.D. degree from Purdue University. He is an Associate Professor with the Department of Electrical, Computer and Energy Engineering, a Fellow of the Renewable and Sustainable Energy Institute, and an Affiliate of the Department of Applied Mathematics, University of Colorado, Boulder. He is also the Chief Scientist and a Distinguished Member of the Research Staff with the National Renewable Energy Laboratory (NREL), Power Systems Engineering Center.



BARRY MATHER (Senior Member, IEEE) received the B.S. and M.S. degrees in electrical engineering from the University of Wyoming, Laramie, WY, USA, and the Ph.D. degree from the University of Colorado at Boulder, CO, USA. During the Ph.D. degree, he was with the Colorado Power Electronics Center (CoPEC). He is the Manager of the Integrated Devices and Systems Group and a Principal Engineer with the National Renewable Energy Laboratory (NREL), Power Systems Engineering Center. His research interests include the development of grid-connected power electronic interfaces to ease renewable generation interconnection, co-simulated transmission and distribution system analysis to investigate system interactions with high levels of distribution-connected generation, and technical standards development. He has more than 90 publications in these research areas and is the author of *High Penetration PV Integration Handbook for Distribution Engineers* which is used as a reference by many utilities world-wide.



AMIRHOSSEIN SAJADI (Senior Member, IEEE) received the Ph.D. degree in systems and control engineering from Case Western Reserve University, Cleveland, OH, USA, in 2016. He is a Research Affiliate with the Renewable and Sustainable Energy Institute (RASEI), University of Colorado Boulder. His main research interests include modeling, planning, dynamics, control, and management of large-scale power systems, including renewable sources and microgrids to enhance the stability, security, and resiliency of energy delivery.